An Evaluation of Supercritical Drying and PEG/Freeze Drying of Waterlogged Archaeological Wood

National Center for Preservation Technology and Training Grant

MT-2210-05-NC-10

Principal Investigator:

Eric Schindelholz

Project Team:

Robert Blanchette
Desmond Cook
Michael Drews
Steve Hand
Benjamin Held
Joel Jurgens
Betty Seifert

Eric Schindelholz
National Park Service
Harpers Ferry Center
P.O. Box 50
Harpers Ferry, WV
25425

Phone: 304-535-5140

The Mariners' Museum

1. Table of Contents

Executive Summary

This study was undertaken to evaluate the physical effects of drying waterlogged archaeological wood using supercritical carbon dioxide as compared to air drying and the popular polyethylene glycol (PEG)/freeze drying method. Previous studies have shown supercritical drying to be a potentially advantageous alternative to current methods of drying waterlogged wood through reduced processing time, minimal shrinkage, and increased success for reversibility.

Samples in the form of blocks and planks of a few centimeters in size were prepared from two archaeological waterlogged wood sources and grouped into three treatment sets: one for air drying, one for PEG/freeze drying, and the other for supercritical drying. Supercritical drying was carried out by replacing water in the wood with methanol, and then removing the methanol in a 250 ml chamber containing supercritical carbon dioxide. Shrinkage was tracked by measuring pins inserted in the samples before and after treatment and by 3D measurement via laser scanning. The scanning allowed a more accurate measure of shrinkage through total volume determinations and 3D distortion comparisons.

Subsamples were taken from randomly selected samples for characterization and treatment. Analyses were carried out to determine the degradation state of the wood prior to treatment. These analyses included density and maximum water content measurements, and the identification and quantification of foreign inclusions in the wood, such as iron corrosion products. The subsamples were examined using low-pressure scanning electron microscopy before and after treatment to determine their state of preservation and the microscopic effects of the imposed treatments.

The wood sources were found to vary in degree of degradation, but all were classified as moderately to highly degraded. Elevated levels of sulfur and ash and very small amounts of iron were found in the subsamples. Overall, PEG/freeze drying gave the best treatment results with virtually no collapse of the wood cell structure and the least amount of shrinkage. Air drying did not produce acceptable shrinkage results. Supercritical drying gave shrinkage results close to the estimated expected shrinkage, but cracking occurred on sets of samples from one of the wood sources. Cracking of these wood source samples also occurred in the air-dried set.

2. Background

Waterlogged archaeological wood is susceptible to major structural collapse and distortion during drying, due to the capillary stress imposed on the cells by liquid surface tension. Current methods used by conservators including slow air drying, liquid solvent replacement, bulking and impregnation, and freeze drying, seek to overcome or minimize capillary stress on wood during drying. Slow air drying and liquid solvent replacement treatments usually result in unacceptable distortion or cracking of the wood. Bulking and impregnation treatments involve diffusing inert materials, such as PEG, into the wood to strengthen or support the cell walls against capillary stress. The rate-limiting step in these treatments is the diffusion of the bulking or impregnation agents into the wood, which may take anywhere from a couple of months to multiple years. Freeze drying avoids capillary stress altogether by eliminating the liquid; however, a cryoprotectant, such as PEG, is needed to prevent damage to the cells during freezing. Consequently, this method suffers from the same long treatment times as bulking and impregnation.

Current methods for drying waterlogged archaeological wood are often time-consuming, unpredictable, expensive, and basically irreversible. For decades, conservators and scientists have been exploring alternative treatment methods in search of a solution to the above-stated problems. On such a mission, Barry Kaye and David Cole-Hamilton of the University of St. Andrews developed the technique of drying waterlogged wood using supercritical fluid (Kaye and Cole-Hamilton, 1994).

By compressing a gas or liquid at elevated temperatures, one can create a supercritical fluid. The latter is basically a cross between a liquid and a gas, possessing certain properties of both, including zero surface tension. Kaye and Cole-Hamilton found that by employing supercritical carbon dioxide (sc-CO_2) fluid to treat waterlogged archaeological wood, drying times could be shortened by a factor of almost 10 and capillary stress problems could be circumvented.

The treatment Kaye and Cole-Hamilton developed is based on solvent replacement. The first step in their treatment involved replacing the water, which is immiscible with supercritical carbon dioxide, with methanol. Above 50^{o}C, methanol is totally miscible with sc-CO_2 within a certain pressure range. The methanol-soaked artifacts were then placed in a chamber and exposed to flowing sc-CO_2 to remove the methanol and dry the object. After the solvent replacement step, the drying process usually took a matter of days to complete (Kaye, Cole-Hamilton and Morphet, 2000).

Using this technique, Kaye and Cole-Hamilton treated over 100 waterlogged archaeological samples and artifacts. They concluded that the treated artifacts exhibited minimal shrinkage and were resilient and environmentally stable. In addition, the treated artifacts had an aesthetically appropriate natural appearance, as their treatments did not add bulking and impregnation agents to the wood (Kaye, Cole-Hamilton and Morphet, 2000). By excluding these agents, supercritical drying is virtually reversible. Teshirogi *et al.* (2002) furthered the pioneering work of Kaye and Cole-Hamilton by publishing the shrinkage results of wood samples treated using the supercritical method. They also developed a mathematical diffusion model for the supercritical drying process.

Although these researchers have examined the physical effects of supercritical drying on waterlogged archaeological wood, their methodology was not completely systematic in terms of sample homogeneity or treatment technique. They did not report on the microscopic effects of supercritical drying on the woods' cellular structure. In addition, direct comparisons between supercritical drying and other treatment types were lacking in their work. This study was designed to address the aforementioned issues and expand upon the work of Kaye and Cole-Hamilton.

3. Introduction

Supercritical carbon dioxide has replaced many liquid organic solvents in industry due to its tunable solvent properties, environmental friendliness, and easily achievable critical parameters. The unique properties of supercritical fluids in general, such as gas-like diffusivity and zero surface tension, make them particularly applicable to the field of conservation. The objective of this research was to methodically evaluate supercritical carbon-dioxide drying of waterlogged wood as compared to wood that has been air-dried and wood that has been treated with polyethylene glycol (PEG) followed by freeze drying. The latter is a method popularly considered by many conservators to give desirable results. Sample shrinkage is the quantitative factor determining the effectiveness of the treatments. Qualitative examination of distortion, cracking, and cellular structure and the evaluation of aesthetic appearance also play a role in the determination.

Three waterlogged archaeological wood artifacts were used for sample material. The deterioration state and homogeneity of deterioration throughout each wood artifact was characterized using low and high-vacuum scanning electron microscopy, pin-testing, and density and maximum water content measurements. Foreign inclusions in the wood, such as iron corrosion products and sulfur compounds were examined using X-ray diffractometry, Mössbauer spectroscopy, and combustion analysis. Total ash content of the wood was also determined.

Thirty-six small block and plank samples were cut from the wood artifacts and treated either by air drying, supercritical drying, or PEG impregnation followed by freeze drying. The technique developed by Kaye and Cole-Hamilton (2000) was used for supercritical drying. A relatively small chamber was used, 250 ml, due to the lack of availability of a larger chamber. This was the limitation factor for sample size. Freeze drying was carried out following a standard procedure used by the Maryland Archaeological Conservation Laboratory that accounts for the species and deterioration state of the wood. Air drying was carried out on a lab bench in ambient laboratory conditions.

Sample shrinkage and distortion was determined by measuring the distance between pins inserted in the samples and by 3D laser scanning before and after treatment. Qualitative examination of all samples before and after treatment was carried out using scanning electron microscopy, 3D scan models, and photographs of the samples themselves.

The experimental procedure is outlined in Figure 1.

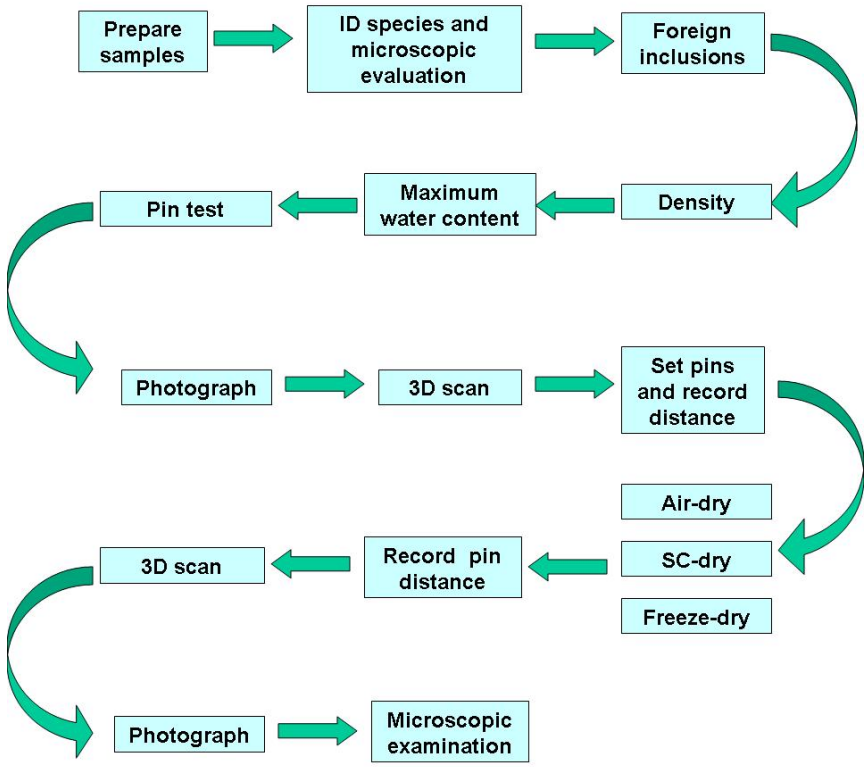

Figure 1. Outline of the experimental procedure

4. Methodology

4.1. Sample Preparation

Samples were prepared from two sources of marine archaeological wood for this study. The first source was comprised of two gunstocks recovered from the wreck of a Civil War blockade-runner, *Modern Greece* (1862), located off the coast of North Carolina. The second source was a board recovered from an early 19th century shipwreck referred to as the Bungay Creek Wreck (18KE-339) found in the Chester River tributary of the Chesapeake Bay.[1] All of the artifacts were found to be rift sawn, meaning the annual rings made angles of 30-60^{o} to the broad surfaces of each piece.

Each source was cut into block and radial-sawn plank samples. Sample size was limited by the size of the supercritical chamber, which had a volume of 250 cm^3. Due to the limited amount of sample material available from each gunstock, one stock was cut into plank samples and the other was cut into blocks. The stock cut into planks is referred to as MG-A, and the stock cut into blocks is referred to as MG-B. The Bungay Creek board was cut into blocks and planks and is referred to as MD.

MG-A and MG-B Preparation

To prepare the two gunstocks, MG-A and MG-B, for sampling, they were first planed down using an electric joiner and planer to achieve a uniform thickness of 2 cm and to remove surface defects such as gouges and excessive marine borer damage.

[1] *Modern Greece* samples were obtained from the North Carolina Branch of Underwater Archaeology. Bungay Creek Wreck samples were obtained from the Maryland Historical Trust.

MG-A was cut into radial-sawn plank samples. This was done by cutting the planed gunstock into 2 x 5 cm blocks using a band saw (Figure 2). The blocks were then culled to remove those that had screw holes or marine borer tunnels that traversed their entirety. The remaining blocks were cut into radial planks measuring 2 x 5 cm and 3-4 mm thick using a fine-tooth backsaw and a miter box (Figure 3). Each plank was labeled using the number of the block from which it was cut followed by a letter designator (e.g. 43a). The planks were culled to remove any that had screw holes or marine borer tunnels. Twelve acceptable planks remained after culling and were assigned to treatments as discussed below.

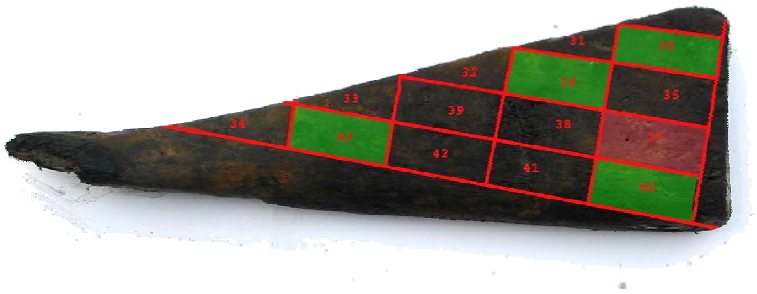

Figure 2. MG-A with overlay of cuts and block assignments. Blocks highlighted in green were used to cut planks. Block 37 (red) was cut into subsamples.

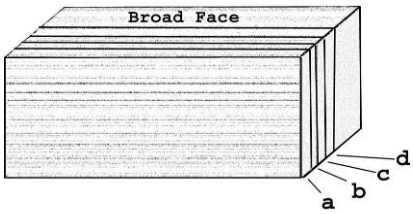

Figure 3. Illustration of planks cut from a block.

Due to the limited amount of sample material that did not have marine borer damage, only one piece of wood, block 37, was suitable for cutting into subsamples. This block piece was cut into five subsamples using a fine-tooth backsaw and miter box (Figure 4). The dimensions of the subsamples were 1 x 1 x 3 cm. Each subsample was labeled using the number of the block followed by a letter designator.

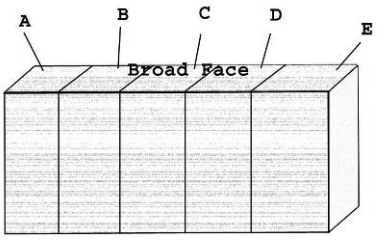

Figure 4. Subsamples cut from block 37.

The other *Modern Greece* gunstock, MG-B was cut into block samples measuring 2 x 2 x 3 cm using a band saw and a fine-tooth backsaw (Figure 5). After cutting, the blocks were sorted and any blocks that contained marine borer tunnels or screw holes were removed. Fifteen acceptable blocks remained after sorting and were assigned to be treated or to be cut into subsamples. The blocks assigned to be cut into subsamples were cut into four pieces measuring 1 x 1 x 3 cm using a backsaw and miter box (Figure 6).

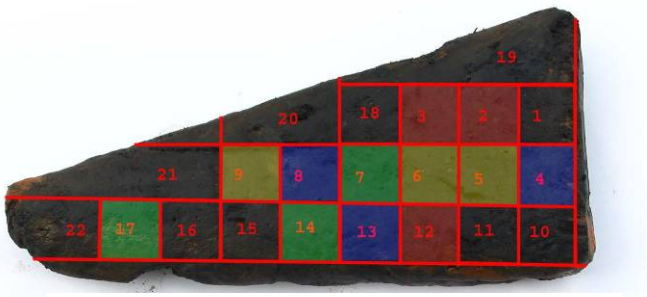

Figure 5. MG-B with overlay of cuts and block assignments. Blue highlighted blocks were cut into subsamples. Green blocks were air-dried. Red blocks were supercritical-dried and yellow were freeze-dried.

MD Preparation

Given the size and shape of MD, both planks and blocks could be cut from it (Figure 7). The original, broad faces of the board were retained (not planed) due to its acceptable flatness and limited surface defects. The board had a thickness of 2 cm. This board was cut using the same tools as those used for MG-A and MG-B.

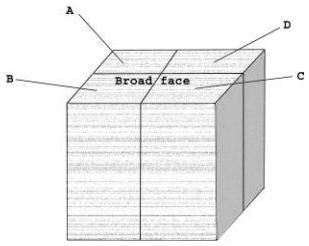

Figure 6. Illustration of subsamples cut from MG-B and MD blocks.

Blocks measuring 2 cm^3 were cut from MD in the same manner as MG-B. After cutting, the blocks were sorted to remove any that had defects such as gouges, nail holes or marine borer tunnels. Seventeen acceptable blocks remained after sorting and were assigned to treatments or to be cut into subsamples. The blocks assigned to be cut into subsamples were further cut into four pieces measuring 1 x 1 x 2 cm in the same manner as MG-B (Figure 6).

Radial-sawn planks, measuring 2 x 5 cm by 3-4 mm thick, were cut from MD in the same manner as MG-A. After cutting, the planks were sorted to remove any that had surface defects, such as gouges, nail holes, or marine borer tunnels. Fifteen acceptable planks remained after sorting.

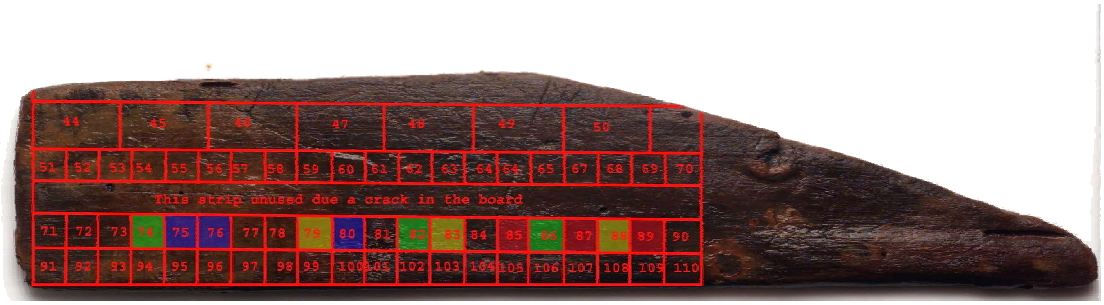

Figure 7. MD with overlay of cuts and block assignments. Blocks highlighted in blue were used for subsamples. Those in green were air-dried. Red blocks were supercritical-dried and yellow were freeze-dried. Blocks 44-50 were cut into planks.

All samples and subsamples were stored in deionized water after preparation.

Sample Assignments

The samples used in this study were grouped into two treatment assemblages– one made up of *Modern Greece* wood (MG-A and MG-B) and the other of Bungay Creek Wreck wood (MD). Nine blocks and nine planks from each wood source comprised each treatment assemblage. Both assemblages were subdivided into three treatment sets, each consisting of three planks and three blocks. Each treatment set was subjected to air drying, freeze drying, or supercritical drying (Figure 8).

All samples in an assemblage were randomly chosen from the pool of prepared samples by drawing numbers and assigned to a treatment set. Block samples, with the exception of MG-A, were also randomly assigned and cut into subsamples.

Two assemblages of twelve subsamples each were produced from MG-B and MD and one assemblage of five subsamples was produced from MG-A (Figures 9 and 10). The lower quantity of MG-A subsamples is due to the lack of sample material as discussed above. For each assemblage, subsamples were randomly chosen by drawing numbers and assigned to a treatment set or to a set that would undergo characterization analyses. Characterization analyses included identifying foreign inclusions and determining density, maximum water content and ash content. Table 5 (Appendix I) lists the assignments of all samples and subsamples utilized for this study.

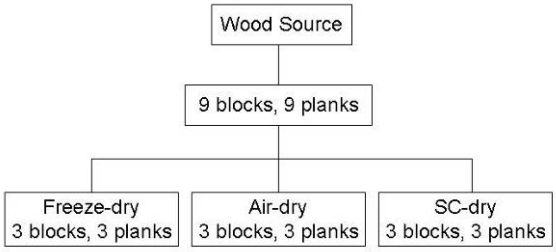

Figure 8. Organization of MG and MD sample assemblages.

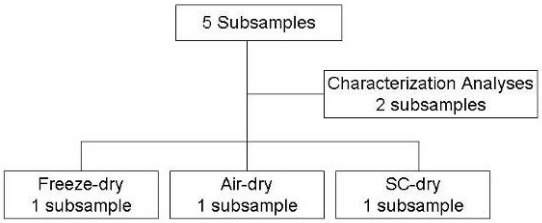

Figure 9. Organization of MG-A subsample assemblage.

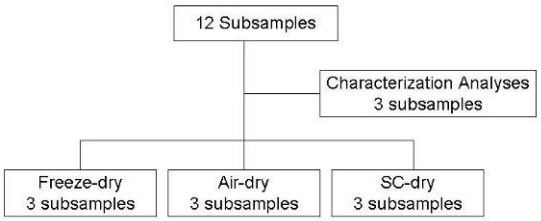

Figure 10. Organization of MG-B and MD subsample assemblages.

Each subsample assigned to undergo characterization analyses was cut in half. One half of each subsample was used to determine density, maximum moisture content (M_{max}) and ash content. The other half was used for foreign inclusion analysis.

Those subsamples that were assigned to a treatment were also cut in half. One half of each subsample was examined in its untreated, waterlogged state and the other half was treated and then examined after treatment.

5. Characterization of Samples

Pin test

All block samples from MG-B and MD along with the blocks from MG-A were subjected to a pin test as described by Christensen (1970). The pin test allowed for qualitative examination and comparison of deterioration variability between the samples and the wood sources. A sewing pin was pushed through the original exterior faces of each sample (i.e. , the faces that were exposed during burial) so that the state of the wood from the exterior to the interior could be determined. The pin was pushed into each sample by hand with even pressure until it went halfway through the sample or it could no longer be pushed in due to sample hardness. If a pin went through the sample with relative ease and little noticeable change in resistance, the sample was determined to be highly deteriorated. Conversely, if the pin could not penetrate the surface of the sample, it was

determined to be relatively undeteriorated. Thus, the ease in which the pin went through the sample was an indication of its deterioration state.

Foreign inclusion analysis

A set of subsamples was analyzed by X-ray diffractometry (XRD) and Mössbauer spectroscopy to identify minerals and iron compounds that had become incorporated in the wood due to their environmental exposure. Carbon-nitrogen-sulfur (CNS) combustion analysis was carried out on the same set of subsamples.

Mössbauer and XRD spectra were recorded of the wet subsamples, which were finely chopped with a stainless steel blade. About 50 mg of the chopped damp wood was sandwiched between two small ½" discs of filter paper and loaded for analysis. Each sample was loaded into a brass sample holder to facilitate easy mounting in the Mössbauer equipment. Spectra were recorded for between 2 and 10 days depending on the signal intensity. The Mössbauer spectra were recorded at room temperature (300^{o} K), and at low temperatures down to 77^{o} K using a Janis 8DT cryostat. For the room temperature measurements, the samples and equipment were aligned and supported on a optical track on a TMC vibration isolation table. For low temperature measurements, the equipment was supported on a Newport Corporation vibration isolation table. A Wissel Mössbauer Transducer was used to oscillate the commercial 25 mCi Co/Rh Mössbauer source, and the velocity range was calibrated using a high purity 7 um thin iron foil at 300^{o} K. A Lake Shore Cryogenics Temperature Controller was used to monitor and control the temperature of each sample inside the cryostat. The Mössbauer spectra were analyzed using *Recoil: Mössbauer Spectral Analysis Software for Windows* (Lagarec and Rancourt), and isomer shifts were referenced to the α-Fe calibration foil.

XRD patterns were collected with a Phillips APD3720 powder X-ray diffractometer using copper radiation. Samples of the wet chopped wood were prepared by compacting approximately 1 gram of material into a standard XRD holder. Patterns were recorded between 10-80 degrees two-theta, using a goniometer step size of 0.02 degrees and a count time of 22 seconds per step. Each pattern was collected over 22 hours with some patterns extended to 44 hours. XRD patterns were analyzed using the standard database of the International Center for Diffraction Data (ICDD).

Carbon-nitrogen-sulfur analysis was carried out using a commercial CNS analyzer (Carlos Erba EA 1108 Elemental Analyzer) calibrated during the batch sample runs using high purity sulfanilamide. The wet wood subsample material, used for the XRD and Mössbauer analyses, was oven dried in air to a constant mass at 45^{o}C for 113 hours in preparation for CNS analysis. The wood material was then chopped finely into triplicate samples, each less than one gram, for CNS analysis. Averages of the CNS results for each triplicate set were utilized for this study.

Ash content

To measure ash content, subsamples were oven dried in porcelain crucibles to constant mass in air at 70^{o}C for 192 hours. They were then weighed on a calibrated analytical balance with an accuracy of 0.01mg. After weighing, the subsamples were placed in a muffle furnace. The temperature was raised to 550^{o}C over 1 hour then stabilized for 22 hours, followed by slow cooling to 100^{o}C over 3 hours. The subsamples were

subsequently re-weighed in their crucibles on the same balance. One blank crucible was included in the procedure as a control.

Density and Maximum Water Content

The density of the subsamples in their untreated and waterlogged state was measured to characterize the deterioration of each wood source. To carry out the density measurements, a set of subsamples was first submerged in a beaker of deionized water and placed under vacuum for 30 minutes to remove any trapped air. Afterward, the density of each subsample was measured by placing it in a 25 ml graduated cylinder ($\pm$0.17 ml tolerance) filled with 10 ml of deionized water. The graduated cylinder was situated on a calibrated balance with an accuracy of 0.1 mg. The mass and volume change after placing each subsample in the cylinder was noted. All subsamples were measured three times, resulting in a maximum standard deviation of 0.011 g/cm^3 for the measurement sets and a coefficient of variation of less than 1%. The averages of the measurement sets were used to calculate the results.

Maximum water content determination was carried out by drying the same set of subsamples measured for density. Each subsample was placed on an individual watch glass after density measurement. The subsamples and watch glasses were then dried in an oven at 105^{o}C for 24 hours. The samples were immediately weighed on the same balance after removal from the oven. The wet and dry masses for each subsample were then used to calculate the maximum water content using the following formula:

where m_m is the wet mass and m_o is the ovendry mass. The specific gravity, G_f, of each

$$M_{max} = \frac{m_m - m_o}{m_o} \times 100\%$$

subsample was determined using the M_{max} and the density results using:

$$G_f = \frac{m_o}{(m_m - m_o) + m_o/G_{so}}$$

where G_{so} is the density of the wood substance. For this study, a density value of 1.5 was used.[2]

The specific gravity of each subsample was then compared to values published by the U.S. Forest Products Laboratory (1974) for the specific gravity of oven-dried, fresh wood for each species. This was done by calculating a percent difference between the specific gravity of the degraded wood and that of oven-dried fresh wood.

Microscopic Examination

Subsamples were examined to evaluate their condition before and after treatment and to identify species. After treatment examination was focused on determining the effects of treatment on the subsamples. For microscopic examination, the subsamples were sectioned by hand with a double-edged razor. They were evaluated in saturated condition

[2] Stamm (1929) has shown that the density of wood substance is relatively constant among different species of wood, and has been measured in the range of 1.50-1.56. Grattan (1987) stated that a G_{so} of 1.5 provides a reliable means of calculating density, although he did state that deterioration may alter the wood substance density.

(before treatment) and after treatment using a Hitachi S-3500N scanning electron microscope (SEM) in low vacuum mode. Some sections were infiltrated with O.C.T. (Tissue Tek®) embedding medium (50% aqueous solution) under vacuum, frozen to -20°C and sectioned with a cryostat freezing microtome. These sections were then air-dried and examined under the SEM for deterioration of the wood structure.

5.2. Treatment

Air drying

Samples and subsamples designated for air drying were dried at 20°C and 50% RH ± 5% for a period of 168 hours. All were weighed before air drying by first placing each one on a dry 5 x 5 cm square piece of paper towel for 15 seconds to remove excess surface water. Each was then immediately placed on a calibrated analytical balance with an accuracy of 0.1 mg. After initial weighing, the samples and subsamples were put on individual plastic weighing trays and weighed every 24 hours during the drying cycle. Drying was considered complete when the mass of the samples became constant between weighing. See Figure 28 in Appendix II for the mass changes during drying.

Supercritical drying

The limited size of the supercritical reactor chamber required subsamples and samples to be run in batches. They were divided into groups based on their geometric characteristics in order to be run in batches. Group assignments are listed in Table 1.

Each group was placed into its own polyethylene container and suspended on a removable sieve. Two hundred milliliters of anhydrous methanol was poured into each container, fully submerging the samples. The methanol in each container was replaced with 200 ml of fresh methanol at one-week intervals. The samples remained in methanol for a period of four weeks.[3] Some batches remained in a few days longer, while in line for supercritical drying. During the final week of methanol exchange, 20 g of dry sodium sulfate was added to the bottom of each container to remove any free water that could have been present in the solution.

Group	Sample ID
1	48a, 36a, 87
2	40c, 49a, 30a, 85
3	49b, 89, 2
4	3, 12
5	1c, 8c, 4c, 80c, 75c, 84c, 37c

Table 1. Group assignments for the supercritical drying procedure.

After the methanol exchange was complete, pins were set in the samples and measured to track shrinkage. The sample and subsample groups were then run in batches through the sc-CO_2 drying system. The sc-CO_2 drying system consisted of an ISCO 260D syringe pump, a Thar R-250 stirred reactor cell and a Thar automated back pressure regulator, as seen in Figures 11 and 12.

To prepare a batch of samples/subsamples for drying, they were wrapped in lint-free polyester cloth wetted with anhydrous methanol and placed into a stainless steel mesh basket. Fifty milliliters of anhydrous methanol was poured into the extraction chamber and the basket containing the samples/subsamples was placed at the bottom of the

[3] See Appendix III for further information on the determination of the methanol exchange end-point.

chamber, submerged in the methanol. This was done to prevent the samples from prematurely drying before they were subjected to the supercritical fluid.

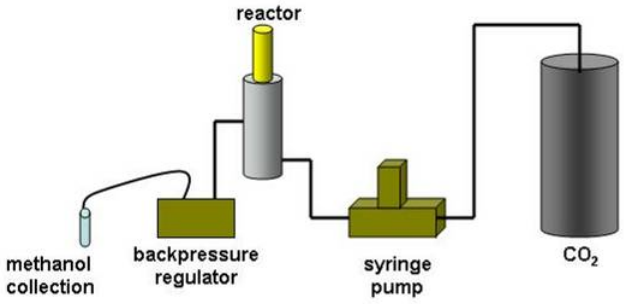

Figure 11. Schematic of the supercritical fluid extraction system.

The chamber was then closed, pressurized with liquid CO_2, the impeller head turned on, and the temperature raised to 45°C. The syringe pump was activated and the pressure stepped to 75 atm and then 100 atm. The temperature was then increased to 50°C with the backpressure regulator set to 0.5 ml/min and the pressure set to a final value of 120 atm. When the system equilibrated at 120 atm and 50°C, the flow was reduced to 0.25 ml/mn for the remainder of the drying process. The operating conditions of 50°C temperature, 0.25 ml/min flow rate, and 120 atm pressure were maintained throughout the course of each drying run using custom-designed software and a computer controller. These parameters were comparable to those used by Kaye and Cole-Hamilton (2000).

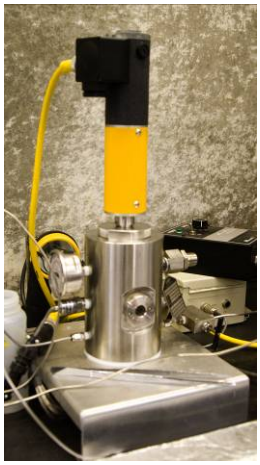

Figure 12. The supercritical reactor chamber and impeller head (yellow).

The completion of methanol extraction indicated the conclusion of the drying run. Extracted methanol was collected in a glass vial in an ice bath at the outlet end of the extraction system (Figure 11). Carbon dioxide flow was maintained for a period of between 30 to 36 hours for each drying run, depending on sample size, until methanol production at the outlet end ceased. The chamber was then allowed to cool and depressurized at a rate of 20 atm/hr for 6 hrs. The treatment was complete at the conclusion of the depressurization cycle. After treatment, the samples were allowed to equilibrate to ambient laboratory conditions of 50% RH $\pm$10% for four days before pin distances were measured.

Freeze drying

Samples and subsamples were placed in an aqueous solution of PEG 400 (Union Carbide) for a period of 15 weeks. They were initially placed in a solution of 10% (w/v) PEG 400 in deionized water and refrigerated at 5°C for a period of 9 weeks. The concentration of the PEG was raised to 20% at week nine and held constant until the end of the fifteenth week.

At the end of week 15, pins were inset in the samples to measure shrinkage. The samples and subsamples were then placed in a freezer at –20°C for 12 hours. After 12 hours, the samples and subsamples were taken out of the freezer and weighed using a calibrated balance with an accuracy of 0.03 mg. They were then placed in a 24” x 48” freeze dryer

(24DX48, Vitris, Inc.) at -28 to -31°C and around 23 millitor to complete the freeze drying process.

The samples and subsamples were periodically weighed during freeze drying to determine the treatment endpoint. This was done by releasing the vacuum on the freeze dryer and taking each sample/subsample out of the freeze dryer, one at a time, to weigh. The temperature of the freeze-dry chamber was held at –20°C while weighing took place. Care was taken not to let the wood thaw while weighing by keeping them out of the freeze dryer for no more than 30 seconds each.

The masses of all samples and subsamples became constant after 33 hours of run time (Figure 29, Appendix II). At this point, the freeze dryer was turned off and the wood in the freeze-dry chamber allowed to equilibrate to the ambient lab temperature and a relative humidity (RH) of 50% $\pm$10% for 72 hours before measuring the pins for shrinkage.

5.3. Sample measurement

Shrinkage was tracked by taking pin measurements and by 3D scanning the samples. The former is a method commonly used in studies pertaining to the evaluation of shrinkage in waterlogged archaeological wood and was used to track radial and tangential shrinkage between certain points on a wood sample. 3D scanning is a technique introduced for use in this study and was successful in accurately tracking distortion in all directions and evaluating total volume of the samples in both their wet and dry (treated) states.

Pin measurement

Shrinkage was tracked by inserting sewing pins in the faces of the samples. Two sets of pins were inserted in the faces of the block samples. Each set tracked either radial (βr) or tangential shrinkage (βt). One set of pins was inserted into one end of each of the planks to measure radial shrinkage. Tangential shrinkage of the planks could not be measured due to their limited thickness. The pin sets were placed in the same faces and areas in all sample sets.

Measurements were carried out using digital calipers with a manufacturer specified accuracy of 0.02 mm. Precision was accounted for by having the same person take the before and after treatment measurements of all samples. Additionally, three measurements were taken for each set of pins before and after treatment, due to the fact that the pins did move some during measurement. The maximum standard deviation of the measurement sets was 0.16 mm. The averages of the measurement sets were used to calculate shrinkage results using the following equation:

$$\text{shrinkage}\,(\%) = \frac{\text{waterlogged dimension - treated dimension}}{\text{waterlogged dimension}} \times 100$$

Average percent shrinkage was calculated for the blocks and planks in each set of air-dried samples. The average air-dried shrinkage values along with the shrinkage values for each sample were used to determine the anti-shrink efficiency (ASE) of the treated samples. ASE expresses a percentage of shrinkage that has been suppressed by a drying treatment as compared to the shrinkage of untreated (air-dried) wood. ASE was calculated using the following formula:

$$ASE = \frac{S_o - S_t}{S_o} \times 100\%$$

where S_o is the shrinkage of the air-dried sample and S_t is the shrinkage of the treated sample.

3D Measurement

3D measurement was carried out using a Leica LR200 coherent laser radar (CLR) scanner. This technology was chosen because of the accuracy needed to identify sample distortion as a result of treatment and the desire for non-contact measurement. The measurement uncertainty of the scanner was $\pm$25 Microns, 2σ at the ranges used for this work.

To set up the measurement system, a control network was first created to maintain coordinate system references. The samples were placed on a set of three pins backed by two first surface optically flat mirrors (Figure 13). The samples were measured directly and by using multiple reflection techniques with mirrors (Figure 14). This allowed for measurement of all sample surfaces without moving the reference coordinate system or the sample.

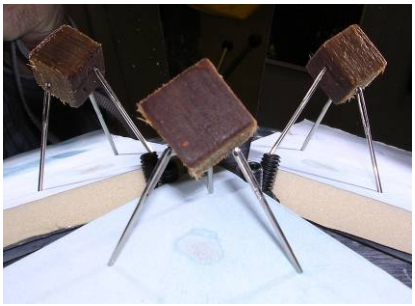

Figure 13. Sample placed on measurement platform in front of mirrors during 3D measurement.

Each sample was scanned before and after treatment. After-treatment scanning was carried out at a relative humidity of 50% $\pm$ 5% after equilibrating the samples to the environment for more than three days. The samples were scanned at 1 mm grid spacing, meaning that a point with xyz coordinates was measured every 1 mm on the sample. The group of points measured for each sample made up a point cloud. Point clouds are the raw xyz point data used to create surfaced models.

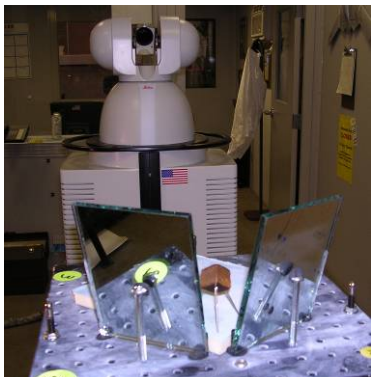

Figure 14. Measurement setup with the CLR scanner in the background.

The before and after treatment point clouds for each sample were edited using Spatial Analyzer software (New River Kinematics) and then exported into a surfacing and inspection software: Polyworks (InnovMetric). The point clouds were meshed together using the best-fit feature in Spatial Analyzer. Each mesh was then polygonized to create a surface in Polyworks. The uncertainty for the surface models was typically $\pm$ 5 micron standard deviation. Holes in the surface, created by shadowing and/or low-quality data, were filled using the Polyworks hole-filling tool (Figure 15). This created a "water-tight" model, from which total volume was calculated.

The total volume of the wet and dry models for each sample was calculated using the Polyworks volume measurement feature. The parameter setting for this feature was set at 100 segments, meaning each sample was sliced or cross-sectioned by the software into

100 segments and the volume calculated from each segment. Total volume shrinkage (βv) and ASE were calculated in the same manner as that for the pin measurements.

The wet and dry models for each sample were compared to each other by placing the dry (smaller) model inside the wet reference model of the same sample. A best-fit alignment algorithm in Polyworks was used to align the orientation of the models together, resulting in a convergence factor below $1x10^{-6}$. After alignment of the wet and dry models, a color comparison map was created using the wet model as the reference model. This resulted in a graphical representation of the three-dimensional shrinkage that each sample underwent as a result of a treatment.

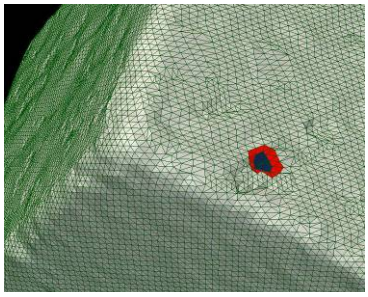

Figure 15. Hole (outlined in red) on the surface of a 3D model before filling.

5.4. Photography

Samples were photographed before and after treatment. Photographs were taken with a Canon EOS20D digital SLR camera.

6. Results and Discussion

6.1. Characterization of Samples

During preparation and the characterization tests, the MG wood appeared more degraded than the MD wood. The MG wood was very soft and spongy and could easily be dented with slight finger pressure. The MD wood was harder, but had a soft and spongy exterior surface. The transverse faces of the MD samples revealed that the soft exterior surface had an orange-brown color, while the inner, harder core was lighter in color (Figure 16). MG samples, on the other hand, had a consistent dark brown appearance (Figure 17)**.** These initial observations suggest that the MG wood was highly degraded while the MD wood was only slightly degraded. The results of the characterization tests, discussed below, confirm these observations.

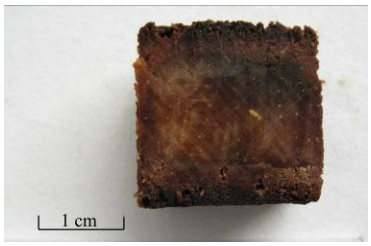

Figure 16. Cross-section of MD block. showing the orange stained exterior and lest stained interior.

Figure 17 Cross-section of MG sample showing homogenous appearance.

Pin Test

Samples within each wood source reacted to the pin test in a similar manner. All samples cut from MG-B could easily be penetrated with the sewing pin. This indicates that the wood was heavily degraded. MG-A samples could be penetrated with the pin, but it was necessary to apply more pressure to reach the middle of the sample. The MG-A samples were likely less degraded than the MG-B samples.

By contrast, a pin could only be pushed 2-3 mm into the MD-A samples before it hit a hard interior core, indicating that these samples are highly degraded for the first 2-3 mm and were only slightly degraded on the interior.

Microscopic Examination

Wood sources MG-A and MG-B were identified as *Juglans* sp. and MD was identified as *Pinus* sp. Although a distinction could not be made during examination, the MG sources were further identified as *J. nigra*, or black walnut, due to the common use of this species for gunstocks during the Civil War period. Likewise, MD is probably *P. strobus,* or eastern white pine, due to the fact that it was recovered from a U.S. shipwreck, ruling out the possibility of other, foreign, species.

The state of deterioration within examined subsamples from each wood source was relatively homogeneous, with the exception of the MD subsamples. MD subsamples had some areas of degradation in which tunneling bacteria attacked the cell walls. These areas were concentrated on the faces of the subsamples that had been exposed during archaeological deposition. Mineral inclusions were not apparent in the wood structures of any of the subsamples during examination.

Although both MG-A and MG-B were recovered from the same shipwreck site, MG-A exhibited much less degradation than MG-B. Similar to MD, MG-A subsamples had areas of degradation but extensive decay was not found. This was consistent for all of the MG-A subsamples examined.

Subsamples from wood source MG-B were the most deteriorated and the extent of degradation was relatively homogenous throughout the subsample set for this wood. MG-B subsamples had highly degraded cell walls leaving only the middle lamella in many regions (Figure 18). In addition to swelling due to water uptake, the subsamples exhibited swelling because of the extensive bacterial degradation that had taken place. The bacteria penetrated the cell walls destroying the cellulose structure and wood strength.

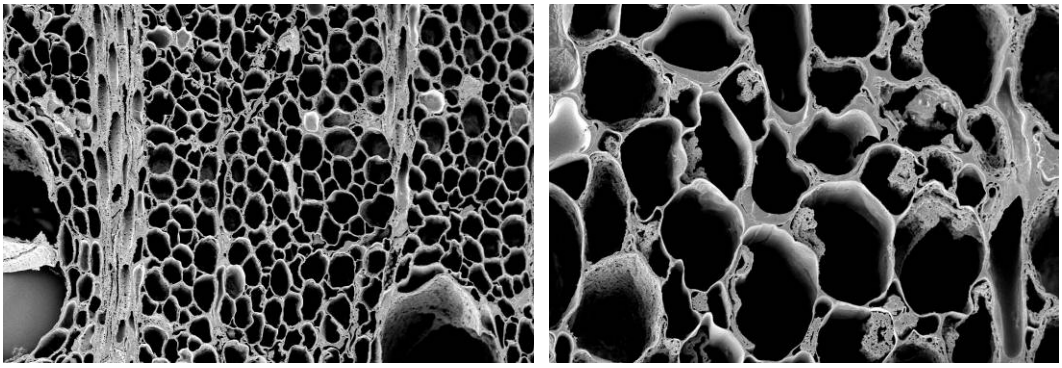

Figure 18. Scanning electron micrographs showing extensive decay in a subsample from the MG-B wood source. Left, cross-section of *Juglans nigra* (x200) showing extensive decay of vessel, fiber and parenchyma cell walls. Right, higher magnification (x900) showing complete degradation of the cell wall leaving only the middle lamella.

Foreign Inclusion Analysis

The results of Mössbauer spectroscopy and X-ray diffractometry analysis are presented in Appendix IV. XRD analysis revealed no detectable concentrations of crystalline substances other than natural cellulose in the wood. The diffraction pattern for each subsample is clearly dominated by cellulose although three different pattern types were observed. Figure 32 in Appendix IV shows that the MD subsamples 84d, 80d and 75d are

nearly identical and are characterized by the standard pattern of natural cellulose (ICDD:03-0289), which has a narrow intense peak at 22.8^{o}. Figure 31shows the patterns of 1d, 4d, and 8d are also similar but are less resolved than in Figure 32. The three broad-peaked patterns are not as similar as for the previous samples. Figure 33 shows the XRD pattern of 37d is clearly cellulose although the background level is much higher than for the other wood samples probably due to its high amount of inclusions as evidenced by ash content, discussed below. These results show that subsamples from the same wood artifacts have similar cellulose diffraction patterns. This may indicate the degree of preservation of the wood from each source.

Mössbauer analysis showed that all subsamples contained iron, but in very small amounts. Long data acquisition times were needed and at times the spectrum was still not resolved due to very low iron content. At room and low temperatures all spectra showed no magnetic ordering, thus eliminating the presence of most iron oxides, as supported by the XRD results. The spectra for all subsamples were similar except for asymmetry between the two main peaks (Figures 34-46, Appendix IV). The spectra showed clear evidence of six iron environments in most samples, and spectral fitting showed the sites to be common for all samples, but with different populations from sample to sample. All iron appears to be ferric form (Fe^{3+}), although assignment to particular compounds is not possible due to the lack of a database of standards for iron in wood in the absence of a defined mineral structure. It is likely that the iron is bound as organo-metallic complexes to the wood and is present in very dilute, non-crystalline form.

The results of combustion analysis are presented in Table 2 and show that all samples have elevated sulfur content. Sulfur content of fresh wood is usually less than 0.1% (Baker, 1983). Seawater contains 0.4% sulfur as sulfate ions. Ranges between 0.1% and 0.4%, therefore, could be expected in archaeological wood recovered from seawater environments. The elevated levels of sulfur in most of the subsamples appear to be the result of sulfate-reducing bacteria in the burial environment, a phenomenon seen in wood recovered from other marine archaeological sites (Sandstrom et al., 2003).

Ash Content

The ash content analysis results are posted in Table 2**.** MG-B subsamples had an average ash content of 7.6%. While the MG-A subsample was measured at 20.1% ash content. The average ash content for the MD subsamples was 9.4%.

Wood Source	Sample	% Ash	%C	%N	%S
MG-B	1d	8.1	49.4	0.6	0.9
	4d	8.9	48.3	0.8	0.9
	8d	5.7	48.1	0.7	0.8
MG-A	37d	20.1	46.6	0.6	1.4
	80d	4.4	50.9	0.3	0.6
MD	84d	4.7	47.1	0.1	0.1
	75d	19.2	49.1	0.4	0.5

Table 2. Subsample ash content and combustion analysis results. All units are percent by dry weight.

The ash content of these subsamples is higher than that found in fresh wood. Most sound woods have an ash content of less than 3% by mass (FPL, 1974). Archaeological woods from waterlogged environments tend to have higher ash content. Mikolajchuk, *et al*. (1989), Grattan (1989), Hoffman (1981) and others have reported up to 20% ash content in archaeological woods recovered from the marine environment. This is due to the increase in concentration of mineral components in the

wood as the organic wood substance degrades and is lost. The influx of inorganic species, such as sulfur and iron into the wood also increases the ash content of the wood (Hedges, 1990).

Maximum Water Content and Specific Gravity

The results of the density, maximum water content, and specific gravity measurements and calculations are displayed in Table 3. The M_{max} value reflects how much water inhabits the void spaces in the wood structure. Degraded wood usually has more void spaces, and thus a higher M_{max} value.

Wood Source	ID	Avg. specific wet density	M_{max}(%)	Conditional S_{og}	Reference S_{og} (oven)*	% S_{og} change
MG-B	1d	1.304	686	0.133	0.55	76
	4d	1.017	671	0.136	0.55	75
	8d	1.002	648	0.140	0.55	75
MG-A	37d	1.003	211	0.360	0.55	35
	37e	1.007	374	0.227	0.55	59
MD	75d	1.054	382	0.223	0.35	36
	80d	1.025	473	0.185	0.35	47
	84d	1.025	479	0.183	0.35	48

Table 3. Results M_{max} and specific gravity determinations.
* reference values for *P. strobus* and *J. nigra* are from (FPL, 1974).

Fresh green wood normally has a M_{max} value of between 40% and 50% (Panshin and Zeeuw, 1980). Fresh *P. strobus* has a heartwood moisture content of 62% while *J. nigra* has a heartwood moisture content of 90% (Hoadley, 1980). As expected, the subsamples groups cut from all three pieces of wood had a M_{max} above that reported for green wood, with the MG-B having the greatest values.

A classification system proposed by De Jong (1977) for waterlogged archaeological wood is regularly cited in conservation literature. This system relates maximum water content with the degree of wood degradation. The MG-B subsamples according to this system are classified as Class I, highly degraded wood. While the MD-A and MG-A subsamples fit into Class II, moderately degraded wood.

Specific gravity measurements were also used to qualify the degradation state of the wood subsamples. Table 3 shows the amount of change or difference between the subsample specific gravities and literature references of oven-dried specific gravities of fresh *P. strobus* and *J. nigra*. The average change of the MG-B subsamples is 75%, while both MD-A and MG-A have similars amount of change, 44% and 47% respectively. This again shows that the MG-B subsamples are much more degraded than the MG-A subsamples

The consistency of M_{max} values indicates how heterogeneously deteriorated each wood source is. The consistency in values obtained from MG-B subsamples indicate that the MG-B wood source is relatively homogenously deteriorated throughout.

The two MG-A subsamples measured had more variance. Given only two subsamples were measured, these values may not reflect the actual homogeneity of the wood

deterioration in the gunstock.. The variance in values of the MD-A subsamples may be explained by the higher measured ash content of 75d, which had the lowest M_{max} value. High ash content equates to a denser subsample, which inversely lowers the M_{max}.

6.2. Effects of Treatment

Visual Observations

Samples treated by the three methods varied in appearance, according to treatment (Figures 47-51, Appendix V). Those that were treated by supercritical drying were lighter in appearance than those that had been air-dried or freeze-dried. The freeze-dried samples were darker and more saturated. The grain of the wood was generally most pronounced in the sc-dried samples.

Three samples, all cut from MG-A, split along the grain boundaries while in treatment. Samples 40b and 40c split in half during handling while in treatment during freeze-drying or sc-drying respectively. Sample 30d, which was air-dried, split as a result of treatment (Figure 19**)**.

Figure 19. Sample 30d split due to air drying.

Cracking was noticed on all MD samples and subsamples that had been air-dried and sc-dried (Figure 20). This was not apparent before treatment or on those that had been freeze-dried. Cracking only occurred on the two original faces of each sample. These faces were found to be highly degraded by pin-testing and microscopic examination, as discussed above. All MD samples and subsamples were further inspected by microscopic examination to determine the cause of cracking, as discussed below.

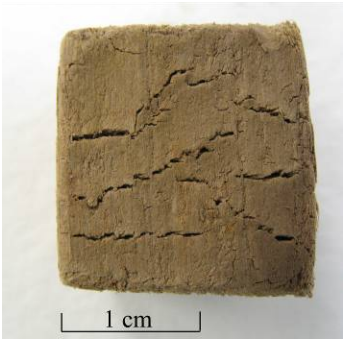

Figure 20. Cracking exhibited by MD sample 89.

All the MG block and plank samples that had been sc-dried or freeze-dried appeared to be in good condition. They did not display any cracking, but it must be noted that, unlike MD, they did not have any original exposed surfaces. Very little shrinkage or distortion of these samples was observed. The air-dried MG samples, by contrast, were found to be extremely shrunken and distorted (Figures 48 and 49, Appendix V).

Shrinkage and distortion

Pin measurements were carried out to determine directional shrinkage (tangential and radial) in the samples. Scan measurements were used to calculate volumetric shrinkage, which was in turn used to determine the ASE of each treatment in this study. The 3D comparison maps created for each sample were used to characterize distortion.

Shrinkage

The shrinkage results for the pin and 3D scan measurements are posted in Tables 6–9, Appendix VI. As is typical for air-dried wood, the pin measurements indicate that tangential shrinkage was roughly twice that of radial shrinkage for the air-dried blocks.

Figures 52–55 in Appendix VI show that this trend is not apparent for those samples that were sc-dried or freeze-dried. Nor does it appear, with the exception of the MG-B freeze-dried samples, that one direction of wood was more stabilized than the other by a certain treatment. These figures also indicate that volumetric shrinkage generally correlates with directional shrinkage.

The volumetric shrinkage measurements give a better overall picture of the shrinkage that occurred for each sample. Volumetric ASE values indicate that freeze drying was most able to suppress shrinkage as compared to supercritical drying, as seen in Figure 56 (Appendix VI). The ASE values of all freeze-dried samples were at or above 80%, with the exception of one sample. The values of sc-dried samples were more diverse, with a range between 44–93%. Over half of the sc-dried sample ASE values were below 75%. Although the freeze-dried samples have higher ASE values than the sc-dried samples, there are no definitive boundaries for ASE values that differentiate a successful treatment from an unsuccessful one.

In fact, a certain amount of normal shrinkage should be expected to occur during the drying of waterlogged wood. This is because wood swells during the process of becoming waterlogged. More specifically, wood swells when it absorbs moisture up to the fiber saturation point (fsp), which is normally around 28% for most woods (Hoadley, 1980). Given the wood artifacts from which the samples were cut probably had a moisture content between 12–15% during their service life, these artifacts likely swelled during archaeological deposition as their moisture content reached fsp, and then beyond.[4] MG-B subsamples were found to have swollen, to some degree, even beyond fsp from deterioration of the cell walls as discussed in section 5.1.

Assuming the wood did not significantly swell beyond the dimensions of its fiber saturation point during archaeological deposition and post recovery, the amount of shrinkage that should be expected to revert the wood to its original dimensions can be estimated using the following formula:

$$\Delta D = D_i \, S\left(\frac{\Delta MC}{fsp}\right)$$

where: ΔD = change in dimension due to shrinkage

D_i = initial dimension

S = total shrinkage percent from green to oven dry in tangential or radial dimension

ΔMC = change in moisture content. For waterlogged wood, 28% is considered the initial moisture content.

fsp = fiber saturation point (28%)

[4] The common equilibrium moisture content range of air-dried lumber in the United States is 12-15% (FPL, 1974). This range was chosen to represent the moisture content of the wood artifacts during their service life in an uncontrolled outdoor environment.

This formula is commonly used to estimate the amount of shrinkage that can occur when sound wood changes from one moisture content to another. Using this equation coupled with shrinkage values for specific species from green to oven-dry published by Hoadley (1980), estimates of the percent shrinkage in the tangential and radial directions for the samples in this study were computed. These estimates were made for wood at fsp (28%) changing to equilibrium moisture content in a laboratory environment of approximately 50% RH (8% MC) and an uncontrolled outdoor environment (12–15% MC). The results are posted in Table 4.

Species	12-15% MC		8% MC	
	β_t (%)	β_r (%)	β_t (%)	β_r (%)
J. nigra	4	3	6	4
P. strobus	4	2	5	3

Table 4. Estimated shrinkage of *J. nigra* and *P. strobus* from fsp to 8% or 12-15% MC.

Due to the fact that the samples were measured for shrinkage after treatment at a relative humidity of around 50%, the estimated shrinkage for that environment was employed as the expected normal shrinkage of the wood during drying. The 12–15% shrinkage estimates prove useful as a reference to the difference between the expected service life dimensions and the dimensions in the laboratory environment. A comparison of measured sample shrinkage with expected normal shrinkage was made (Figures 57–60, Appendix VI). In general, the air-dried samples exceeded their expected shrinkage to an amount reflecting the degradation level of the wood source from which they originated. Samples from MG-B, the most degraded wood source, shrank by the greatest amount. MG-A samples shrank less than MG-B, followed by the MD samples. The MD planks shrank the same as the estimated amount of 3% in the radial direction, but still were severely shrunken as indicated by volumetric measurements.

Samples treated by supercritical drying, with the exception of the MG-A samples, mostly exhibited shrinkage closest to the estimated normal shrinkage values as compared to the other treatments. The average shrinkage of the MD planks that were freeze-dried and sc-dried was comparable. Freeze-dried MG-A planks were closest in shrinkage to the estimated value as compared to the sc-dried planks. The MG-A results, however, are somewhat skewed given one plank in each set broke during treatment and could not be measured.

Distortion

The 3D comparison maps produced from scanning were used to characterize and compare the distortion that occurred from the treatment of each sample (Appendix VII). Shrinkage is seen to have occurred primarily in the tangential and radial directions of the samples, with very little if any shrinkage occurring in the longitudinal direction.

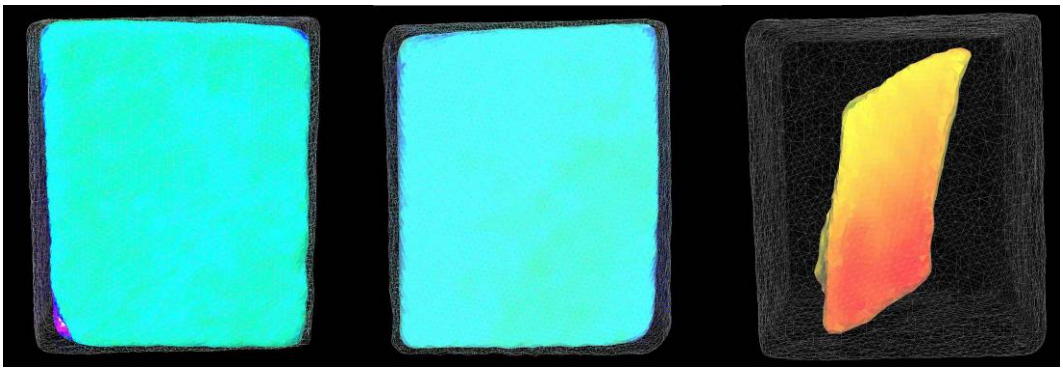

Figure 21. Comparison of transverse faces of 3D comparison models of treated MG block samples. The grey wire frame model is the wet sample and the colored solid model is the treated sample. Left freeze-dried sample 5. Center sc-dried sample 12. Right air-dried sample 14.

Diamonding is the characteristic distortion feature of all block samples. Diamonding, as seen in Figure 21 occurred due to shrinkage differences in the radial and tangential directions of the wood. This is typical for samples of this cut (Figure 22). It was found that the more volumetric shrinkage that occurred, the more pronounced the diamonding was. Diamonding of the freeze-dried MD samples, having shrunk only an average of 1%, was barely noticeable. Some degree of diamonding should be acceptable, given that the samples were expected to exhibit some amount of normal shrinkage during drying from a waterlogged state. It must be kept in mind that these samples were not original artifacts themselves, but cut from larger artifacts. Distortion of the samples in the context of the overall artifact may have conformed to the original dimensions and shape of the artifact.

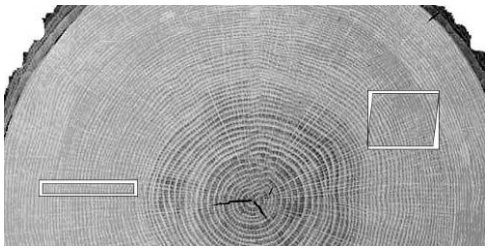

Figure 22. Orientation of subsamples in context of a log. with expected warp as a result of drying.

Collapse occurred as a result of air drying on the original (exposed) faces of two MD blocks, 86 and 82 (Figure 23). The collapse was in the form of depressions on each side of their original faces and 1.5–2 mm deep. This collapse corresponds roughly to the thickness of the highly degraded surfaces of these pieces and the cracking that occurred (Figure 20), clearly showing that the degraded areas lacked structural integrity.

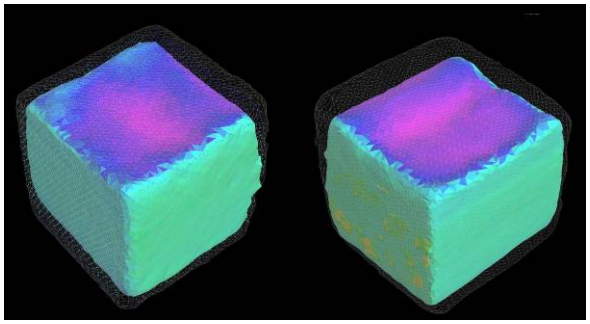

Figure 23. 3D comparison maps of air-dried samples 86 (left) and 82 (right) highlighting collapse of degraded original surfaces. The purple-blue areas, the degraded surfaces, have collapsed between 3-4 mm.

Warping occurred on two planks from MG-A. Samples 30d and 30G were air-dried and significantly shrank and cupped during drying (Figure 70, Appendix VII). The lack of apparent warping in the remainder of the samples is likely due to the fact that they were

radially cut.

Microscopic Examination
Subsamples were examined to determine the effects each treatment had on the various wood sources. Furthermore, the cracking found on the air-dried and sc-dried MD samples was further examined to determine the cause of this undesirable effect.

Air-dried
The air-dried MG-A (*Juglans* sp.) subsamples showed wood cell structures that were well preserved and resembled the original wood structure as shown by the SEM images in Figure 24**.** The MD (*Pinus* sp.) subsamples exhibited a well-preserved interior wood structure and a collapsed and deformed exterior, which was confined to the highly deteriorated original exposed faces of the subsamples. MG-B exhibited severe alteration and collapse of the cell structure upon air drying. This failure of wood structure and strength can be attributed to the more extensive decay in MG-B as discussed above.

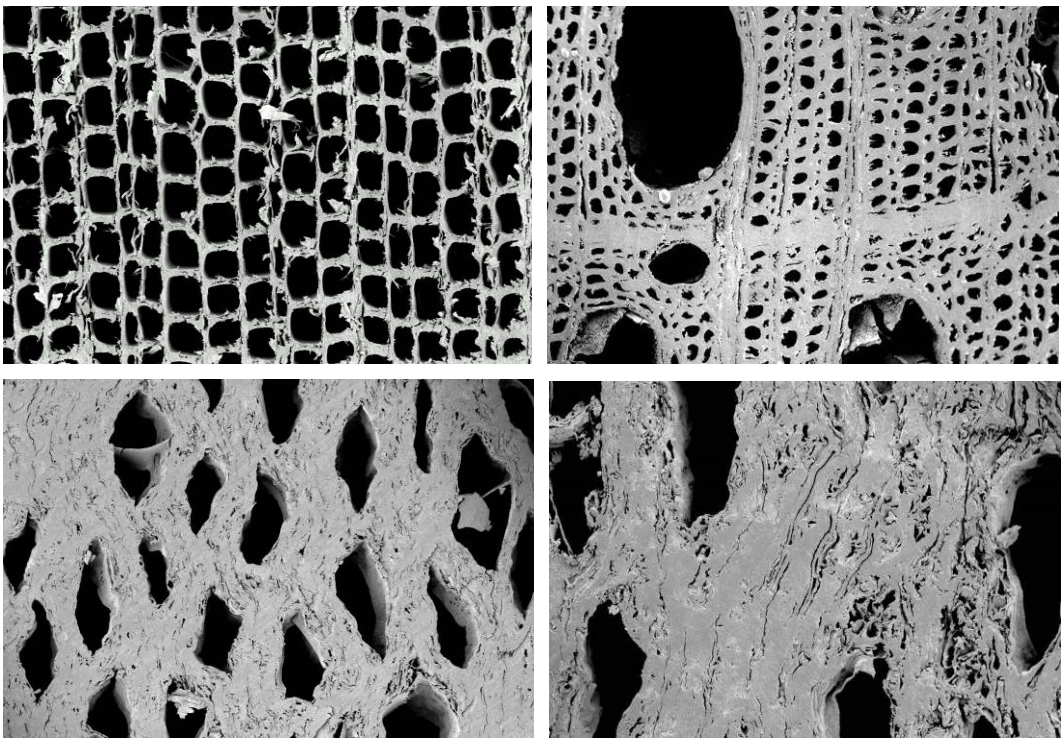

Figure 24. SEM micrographs of cross-sectioned air-dried subsamples from all wood sources. Upper left, MD (*Pinus* sp.) sample showing intact wood structure from an area that had little to no decay (mag. x200). Upper right, MG-A (*Juglans* sp.) sample showing intact wood structure (x200) from a decay free area of the wood. Lower left, MG-B (*Juglans* sp.) sample showing dramatic alteration and distortion of wood cell structure (x100). Lower right, higher magnification (x200) of sample MG-B showing complete collapse of the cell structure. The large vessel elements are still visible, but cells have been distorted. All cells between the vessels are collapsed and appear fused together in an amorphous mass.

Freeze-Dried
Those subsamples treated by freeze drying exhibited the best overall condition of the wood cell structure when compared to the other two treatments. Microscopic examination

of the cross-sections prepared from all freeze-dried subsamples exhibited good preservation of cell structure and overall condition. The PEG appeared to have infiltrated the bacterial cavities present in the secondary walls of the degraded wood providing stability by holding the decayed wood structure together (Figure 25). This is in contrast to the air-dried and sc-dried subsamples.

Observations indicate that the PEG infiltrated the subsamples in a uniform manner. Although abundant tyloses were observed, which could affect PEG infiltration, in the MG-A subsamples, the permeability of these decayed subsamples was sufficient to allow good penetration.

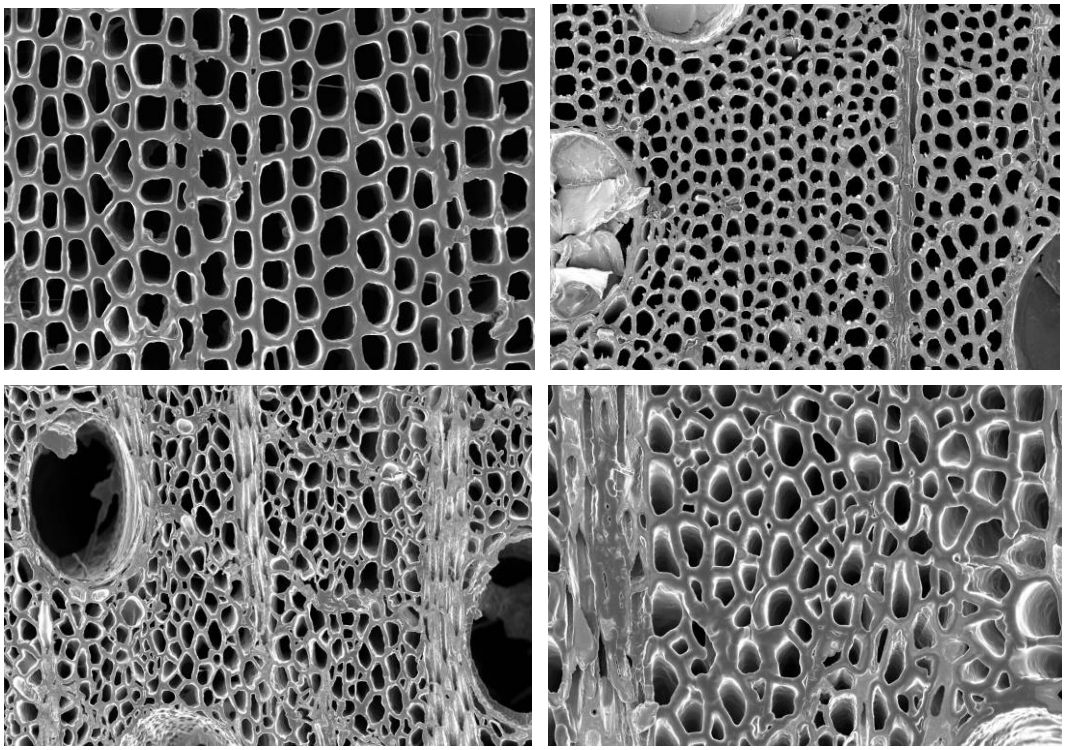

Figure 25. SEM micrographs of transverse sections of wood freeze-dried from all wood sources (x200). Upper left, MD sample showing intact wood structure; Upper right, MG-A sample showing unaltered cell structure of *Juglans* sp. Lower left, MG-B sample of *Juglans* sp. showing disrupted wood structure in area with extensive decay. Lower right, freezing microtome cross section of an MD sample showing extensive decay where only the middle lamella region of the cell wall is intact. The extremely weak and fragile condition of the cell wall is clearly evident.

Supercritical-Dried

The supercritical-dried subsamples exhibited effects from treatment similar to the air-dried subsamples. MD and MG-A subsamples showed a relatively unaltered wood structure from the wet state (Figure 26, upper left and upper right). The subsamples were found to be brittle and weak during preparation, but overall maintained their original structure.

Subsamples from wood source MG-B (Figure 26, lower left), however, exhibited areas of extensive collapse and varied significantly from other wood sources treated by supercritical drying. The supercritical treatment technique did not prove sufficient in

preserving the cell structure of the wood (Figure 26**,** lower left). Although it is difficult to explain the cause of this collapse without further investigation, it is possible that it could have been caused by osmotic pressure on the cell walls during the methanol-water exchange process. Figure 26 (lower right) shows, however, that the supercritical treatment technique does quite well in some respects to preserve the degraded cell wall. As the micrograph shows, the cell wall is almost completely degraded by tunneling bacteria leaving only the middle lamella. This extensive attack greatly compromises all wood strength properties.

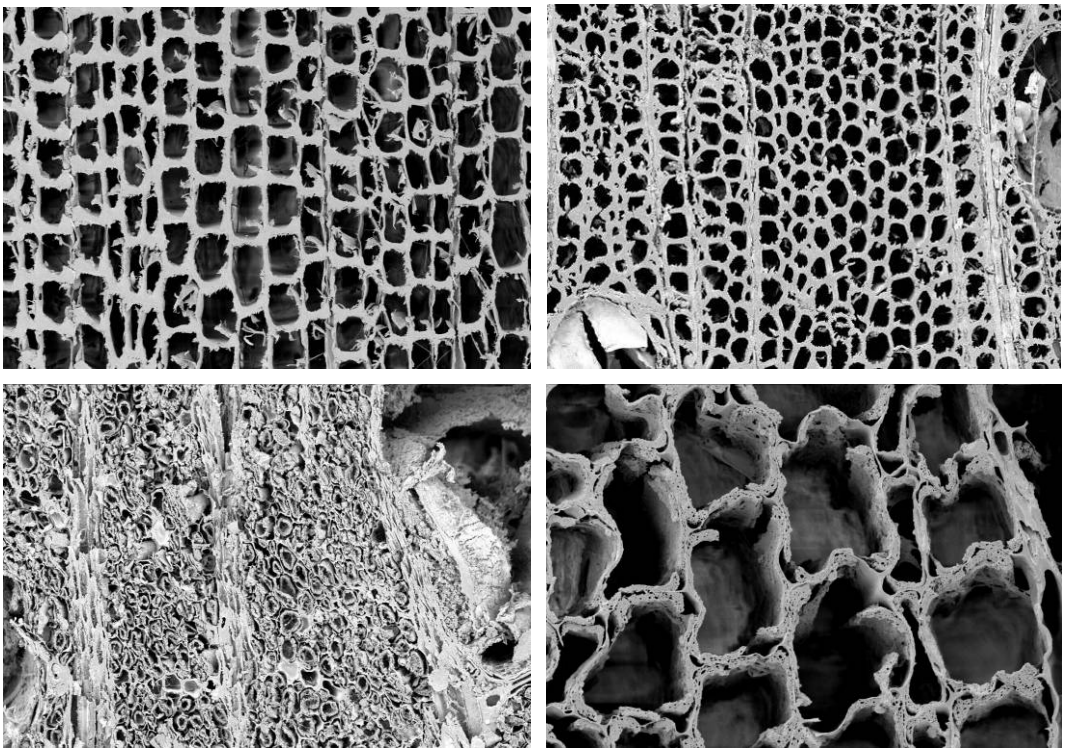

Figure 26. SEM micrographs of transverse sections of wood supercritical-dried from all wood sources (x200). Upper left, MD sample showing intact wood structure; Upper right, MG-A sample showing unaltered cell structure of *Juglans* sp.; Lower left, MG-B sample of *Juglans* sp. showing disrupted wood structure in area with extensive decay; Lower right, freezing microtome cross section of an MD sample showing extensive decay where only the middle lamella region of the cell wall is intact. The extremely weak and fragile condition of the cell wall is clearly evident.

Cracking

Only the air-dried and sc-dried MD samples and subsamples displayed cracking on their exterior surfaces after treatment. This cracking was limited to the two original faces of the subsamples and samples, as discussed above. The SEM micrographs in Figure 27 show that in areas of no cracking (left) cell structure is normal with very little degradation. Alternatively, in areas where cracking has occurred (right), greater degradation is present. The loss of strength is apparent by the distorted shape of the cells, and many cell walls have collapsed. This extremely weak cell structure defining the ease with which the cells can break is the likely cause for cracking.

In the drying process, the tension on the outer degraded cell walls was apparently too great and cracks subsequently formed. The tension may have been formed by the differential shrinkage between the less-degraded interior and more degraded wood surface. Freeze-dried samples and subsamples did not have this problem associated with them due to the PEG infiltration into the degraded cell walls which provided a stabilizing effect and probably lessened the shrinkage differential.

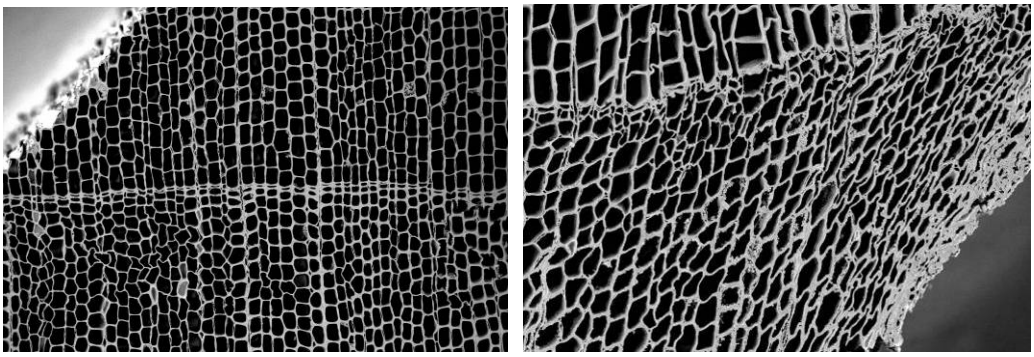

Figure 27. SEM micrographs of cross-sections of an air-dried subsample (MD) with cracks. Left, section from a side of the sample without cracking (x80). The cell structure of this uncracked region is normal and intact. Right, view from a face of the sample with cracking. Cells in this area are more degraded and collapsed (x150).

7. Conclusion

The objective of this research was to methodically evaluate supercritical carbon-dioxide drying of waterlogged wood as compared to wood that has been air-dried and wood that has been treated with polyethylene glycol (PEG) followed by freeze drying. Three waterlogged archaeological wood artifacts were used as sample material in the study. Small block and plank samples, 36 in all, were cut from the wood along with subsamples. Sets of samples and subsamples were subjected to air drying, freeze drying, or supercritical drying. Some subsample sets were used to characterize the wood sources.

Characterization of the wood sources used for sample material in this study included pin-testing, foreign inclusion analysis, density, and maximum water content determination and microscopic examination. The wood sources were identified as *Juglans nigra* (*Modern Greece*) and *Pinus strobus* (Bungay Creek Wreck). The two artifacts, MG-A and MG-B, comprising the *Modern Greece* wood source were found to be homogenously deteriorated. MG-B was found to be most degraded with areas of extensive loss of vessel, fiber, and parenchyma cell walls and an average M_{max} of 668%. The MG-A wood was found to be only slightly deteriorated with an average M_{max} of 290%. The MD wood source exhibited highly degraded areas on its faces that were exposed to the archaeological environment and a relatively sound core. Foreign inclusion analyses found that wood from all artifacts exhibited elevated levels of ash and sulfur. X-ray diffractometry and Mössbauer spectroscopy were not able to detect any crystalline substances or corrosion products in the samples except cellulose.

Treatment effectiveness was determined by macroscopic and microscopic examination, shrinkage measurements, and distortion evaluation. Samples varied in appearance according to treatment. The supercritical-dried samples were generally lighter and more

natural in appearance with more visible grain than the freeze-dried samples. The freeze-dried samples had a darker, saturated appearance, while the air-dried samples were somewhere in between. All of the MD samples that were sc-dried or air-dried exhibited cracking on their highly deteriorated exposed faces. This is may be due to differential shrinkage between the highly degraded surfaces and the less degraded interior. Samples that were air-dried were visibly shrunk and distorted.

Shrinkage measurement results favored freeze drying and supercritical drying over air drying. Volumetric shrinkage generally correlated with directional shrinkage. Three-dimensional comparison models show that longitudinal shrinkage was minimal or non-existent for all samples. The volumetric shrinkage outcomes showed that freeze drying resulted in the least amount of sample shrinkage, followed by supercritical drying, and then air drying. Normal shrinkage as a result of drying from fsp to 8% MC was estimated for these samples. The air-dried samples exceeded their estimated shrinkage according to the degradation level of the wood source from which they originated with the MG-B samples having shrunk the greatest amount. Supercritical-dried samples exhibited values closest to the expected shrinkage as compared to freeze drying, with the exception of the MG-A samples.

Air-dried samples were found to be more distorted than those treated by freeze drying or supercritical drying. Diamonding was characteristic of all block samples, being less apparent on those samples that exhibited the least amount of shrinkage. Collapse of the highly degraded faces of two of the MD block samples occurred as a result of air drying. Warping was only apparent on the air-dried MG-A plank samples. The small number of warped plank samples is likely due to the fact that they were radially cut.

Examination of the treated subsamples using low-vacuum scanning electron microscopy found that the freeze-dried subsamples from each source exhibited the best overall condition of wood structure as compared to the other treatments, with the exception of those from MG-A. Wood structures of the MG-A subsamples treated by all methods remained relatively unchanged from their wet state. Air-dried and sc-dried MG-B subsamples exhibited extensive areas of collapse. A possible cause for collapse of the sc-dried MG-B subsamples is that the osmotic pressure, created by immersing the waterlogged wood in pure methanol during the solvent exchange process, was great enough to cause the degraded cells to collapse. MD subsamples subjected to any of the treatments exhibited a well-preserved core. The highly degraded faces of the MD samples collapsed and cracked upon air drying and supercritical drying due to the weak condition of the cell walls. Freeze drying was able to stabilize the highly degraded areas through infiltration of the bacterial cavities in the secondary cell walls of the structure.

In general, freeze drying performed better than the other treatments in the study. Samples that were freeze-dried exhibited little shrinkage or collapse of the cell walls and an acceptable, albeit dark, appearance. Air-dried samples exhibited unacceptable shrinkage, cracking, and, in some cases, warping. Supercritical drying was able, in most cases, to maintain shrinkage close to the estimated normal values for all samples and produced samples that had a natural appearance. Supercritical drying of the MD wood samples did not produce acceptable results, due to the cracking that occurred on the weathered surfaces of the samples. Cracking was likely due to the inability of the extremely degraded nature of the wood structure on the weathered surfaces to support itself during

drying. Microscopic examination made it clear that PEG was able to stabilize these highly degraded areas.

The results of this study show that the supercritical drying technique developed by Kaye and Cole-Hamilton is not appropriate for all types of wood. Cracking was the major cause of failure for the technique in this study. For those woods able to be successfully treated by sc drying, such as the MG samples, the technique still offers advantages of quick drying times, acceptable shrinkage, natural appearance, and treatment reversibility. It is recommended that the conservator wishing to use supercritical drying for these reasons first test samples of the wood he/she plans to treat, if possible, before subjecting it to treatment.

8. Future Work

The results of this study show the need for further testing of supercritical drying for waterlogged wood. Foremost, additional and varied waterlogged archaeological wood sources should be tested for their compatibility to supercritical drying in terms of cracking and shrinkage as compared to air-drying and freeze-drying. Particular attention should be given to woods with degraded surfaces and relatively undegraded interiors. Modifications to the supercritical technique used in this study may aid in curbing cracking similar to that which had occurred in this study. The methanol exchange process should be examined closely to determine whether or not immersing degraded waterlogged wood in pure methanol can cause collapse of the wood cells. It should be recognized that this study was conducted on a pilot scale and did not utilize whole artifacts as sample material. A follow-up study that utilizes a much larger chamber and whole artifacts as samples would allow for direct assessment of the effects of supercritical drying on waterlogged artifacts.

9. Acknowledgments

Funding from the National Center for Preservation Technology and Training and The Mariners' Museum supported this study. Thanks are due to the following people and organizations for their gracious contributions to this work:

Jason Hemmer and Amanda Wagner of Clemson University for carrying out the supercritical drying; Howard Wellman of the Maryland Archaeological Conservation Laboratory for aiding in the set-up of the freeze dryer; Rick Uhal of Maglev, Inc. for carrying out scanning of the samples; David Velinsky of The Academy of Natural Science for carrying out CNS combustion analysis; Nathan Henry of the North Carolina Underwater Archaeology Branch for donating the *Modern Greece* sample material; Bruce Thompson and Susan Langley of Maryland Historical Trust, for donating sample material from the Bungay Creek Wreck; Alan Levitan and Larry Bowers of the National Park Service for helpful suggestions during the preparation of this manuscript; The Mariners' Museum, Conservation Department for editing the manuscript.

References

Baker, A.J. 1983. Wood fuel properties and fuel products from woods. In *Fuelwood Management and Utilization Seminar Proceedings*, 14-25. East Lansing, MI: Michigan State University.

Christensen, B. 1970. *Conservation of Waterlogged Wood in the National Museum of Denmark*. Copenhagen: National Museum of Denmark.

De Jong, J. 1977. Conservation techniques for old waterlogged wood from shipwrecks found in the Netherlands. In *Biodeterioration Investigation Techniques*, ed. A. Walters., 295-338. London: Applied Science Publishers.

FPL. *See* U.S. Forest Products Laboratory.

Grattan, D.W. 1987. Waterlogged wood. In *Conservation of Marine Archaeological Artifacts*, ed. C. Pearson, 55-67. London: Butterworths.

- . 1989. International comparative wood treatment study. In Conservation of Wet Wood and Metal: Proceedings of the ICOM Conservation Working Groups on Wet Organic Archaeological Materials and Metals, ed. I. Macleod, 163-192. Perth, WA: Western Australian Museum.

Hedges, J. 1990. The chemistry of archaeological wood. In *Archaeological Wood:Properties, Chemistry and Preservation*, eds. R. Rowell and J. Barbour, 111-140, Washington, D.C.: American Chemical Society.

Hoadley, B. 1980. Understanding Wood: A Craftsman's Guide to Wood Technology. Newton, Connecticut: Taunton Press.

Hoffman, P. 1981. Chemical wood analysis as a means of characterizing archaeological wood. In *Proceedings of the ICOM Waterlogged Wood Working Group Conference*, ed. D.W. Grattan, 73-83. Ottawa: ICOM Committee for Conservation, Waterlogged Wood Working Group.

Innovmetric. Polyworks [computer software]. Quebec City: Innovmetric.

Kaye, B., D. Cole-Hamilton and K. Morphet. 2000. Supercritical drying: a new method for conserving waterlogged archaeological materials. *Studies in Conservation* 45: 233-252.

Kaye, B. and D. Cole-Hamilton. 1994. Novel approaches to the conservation of wet wood. In *A Celebration of Wood*, ed. J.A. Spriggs. York: York Archaeological Wood Centre.

Lagarec, K. and D. Rancourt. Mössbauer: Spectral Analysis Software for Windows, Version 1.0. [computer software]. Ottawa: University of Ottawa.

Mikolajchuk, E. et al. 1989. Examination of waterlogged archaeological oak wood. In Conservation of Wet Wood and Metal: Proceedings of the ICOM Conservation Working Groups on Wet Organic Archaeological Materials and Metals, ed. I. Macleod, 95-108. Perth, WA: Western Australian Museum.

New River Kinematics. Spatial Analyser. [computer software]. Williamsburg: New River Kinematics.

Sandstrom, M. et al. 2003. The sulphur threat to marine archaeological artefacts: acid and iron removal from the *Vasa*. In proc. of *Conservation Science 2002*, eds. J. Townsend, K. Eremin, and A. Adriaens, 79-87. London: Archetype Publications.

Stamm, A.J. 1929. Density of wood substance, absorption by wood, and permeability of wood. *Journal of Physical Chemistry* 33: 398-414.

Teshirogi, Miho et al. 2002. Conservation treatment of water-logged wood with supercritical carbon dioxide. In *Proceedings of the 8th ICOM Group on Wet Organic Archaeological Materials Conference*, eds. P. Hoffman et al., 371-377. Bremerhaven: Deutsches Schiffahrtsmuseum.

Panshin, A.J. and Carl de Zeeuw. 1980. *Textbook of Wood Technology: Structure, Identification, Properties, and Uses of the Commercial Woods of the United States and Canada.* New York: McGraw-Hill Book Company.

U.S. Forest Products Laboratory. 1974. *Wood Handbook: Wood as an Engineering Material.* Washington, D.C.: U.S. Government Printing Office.

Wagner, A. 2005. Evaluation of supercritical drying of archaeological wood. Undergrad. thesis, Clemson Univ.

Appendix I: Sample and Subsample Assignments

Wood Source	Treatment			Characterization Analyses
	Freeze	SC	Air	
MG-A				
Planks	43a 40b 40f	30a 40c 36a	30d 43b 30g	
Subsamples	37b	37c	37a	37d,e
MG-B				
Blocks	5 6 9	12 2 3	14 7 17	
Subsamples	1b 4b 8b	1c 4c 8c	1a 4a 8a	1d 4d 8d
MD				
Planks	48c 49c 49f	48a 49a 49b	49d 48b 49e	
Blocks	88 79 83	89 85 87	82 74 86	
Subsamples	80b 75b 84b	80c 75c 84c	80a 75a 84a	80d 75d 84d

Table 5. Sample and subsample assignments.

Appendix II: Mass Changes of Samples during Treatment

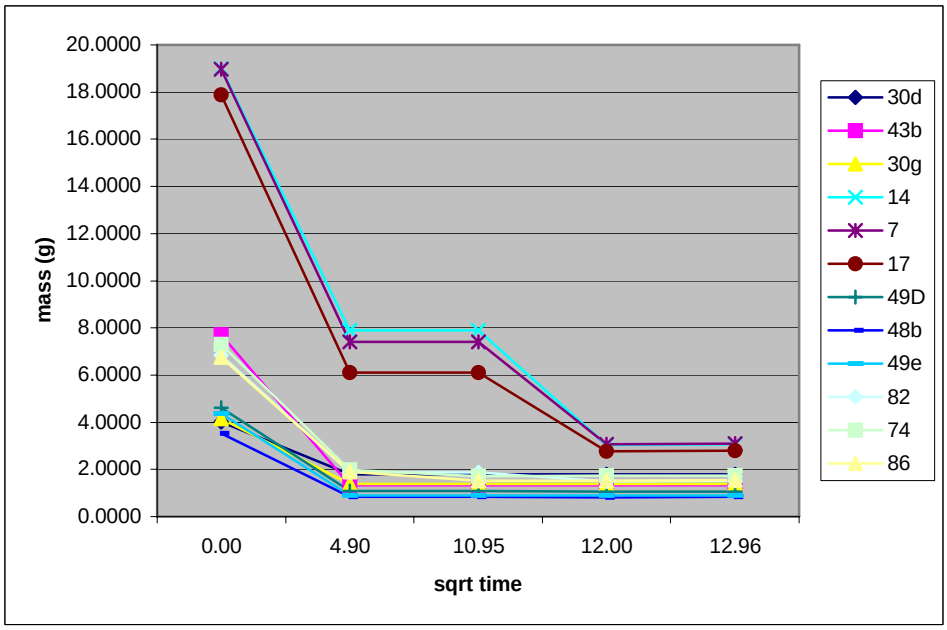

Figure 28. Mass loss of samples and subsamples versus the square root of time during air drying and equilibration after treatment.

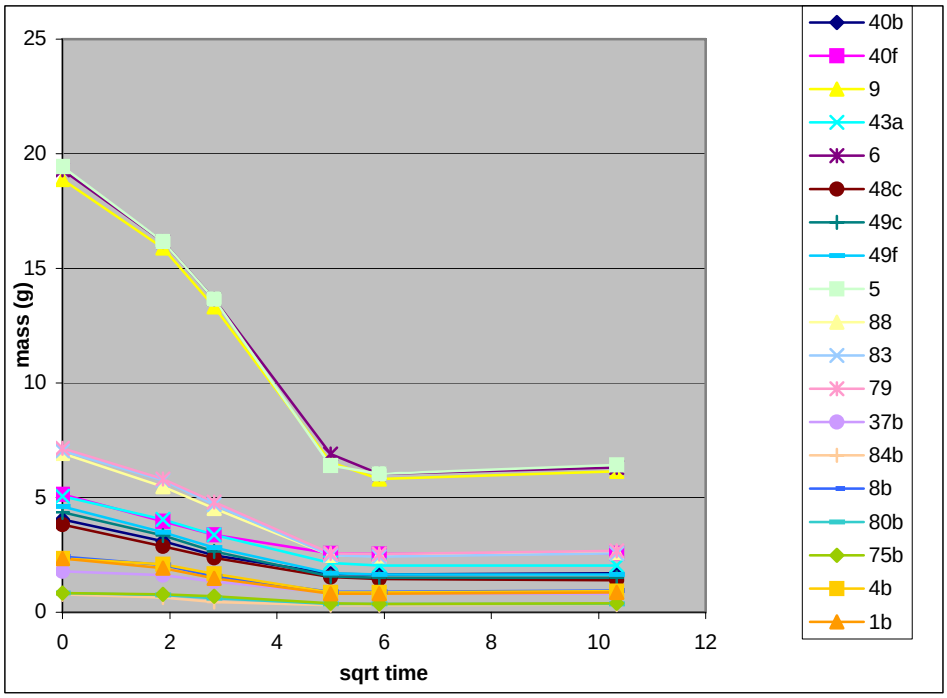

Figure 29. Mass loss of samples versus the square root of time during freeze drying.

Appendix III: Methanol Endpoint Determination Pilot Study

Four weeks was determined to be the end-point of the methanol exchange based on a pilot experiment carried out to determine the water-methanol exchange rates of the source wood in methanol (Wagner, 2005). The pilot experiment involved submerging two sets of samples in separate anhydrous methanol baths for up to four weeks. The samples were cut from the MG and MD wood sources and were of the same size used for this study. The methanol baths were changed out with fresh anhydrous methanol every seven days. The used methanol solutions for every week were analyzed using Karl-Fischer titration to determine water concentration. Water content in the methanol solution was measured at less than 5% after two weeks and under 1% after weeks three and four. A constant reading of less than 1% water content signaled the endpoint of the methanol exchange process. Thus, four weeks was seen as a safe endpoint for the methanol exchange in this study.

Appendix IV: Mössbauer and XRD Results

X-Ray Diffraction Results

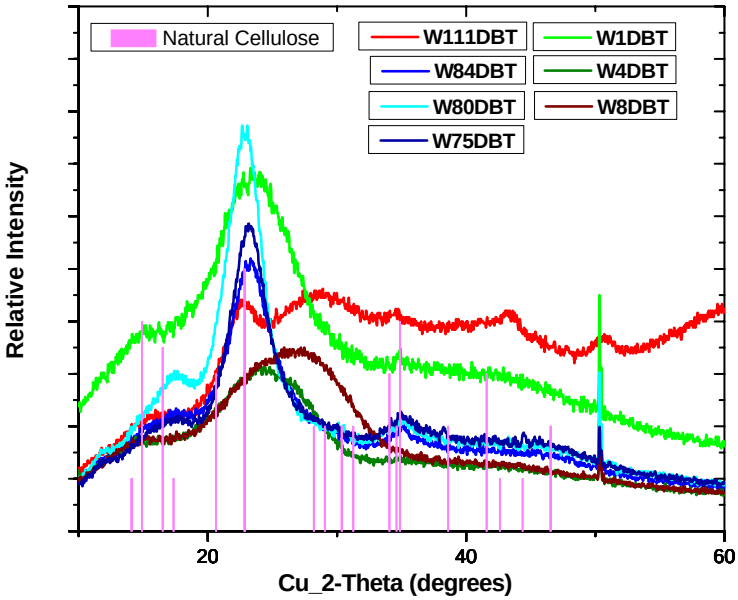

Figure 30. XRD patterns of seven subsamples referenced to natural cellulose.

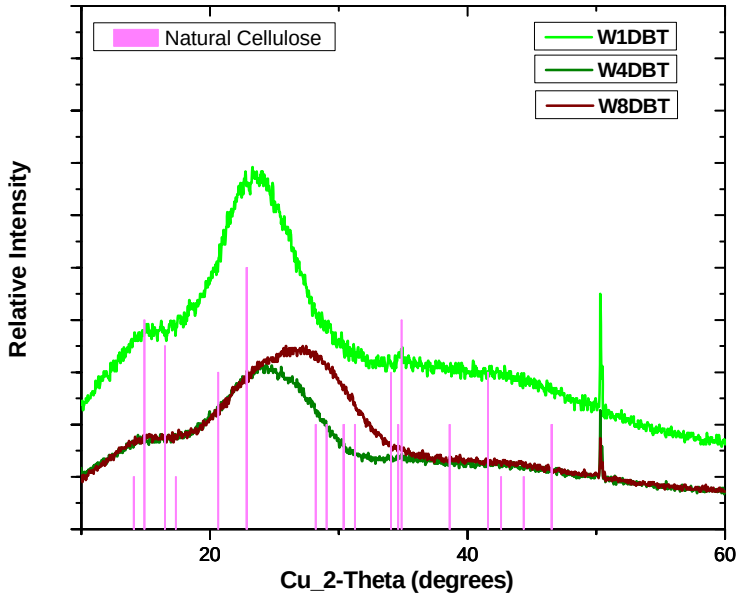

Figure 31. XRD patterns of MG-B subsamples referenced to natural cellulose.

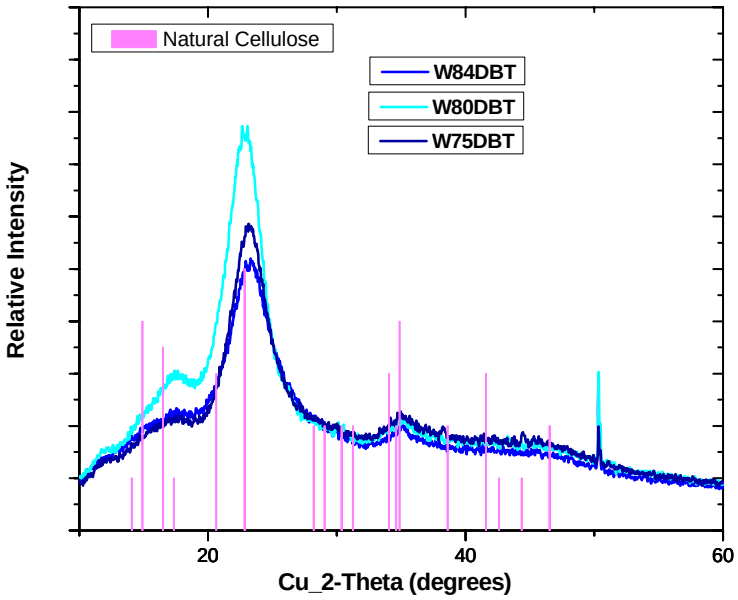

Figure 32. XRD patterns of MD subsamples referenced to natural cellulose.

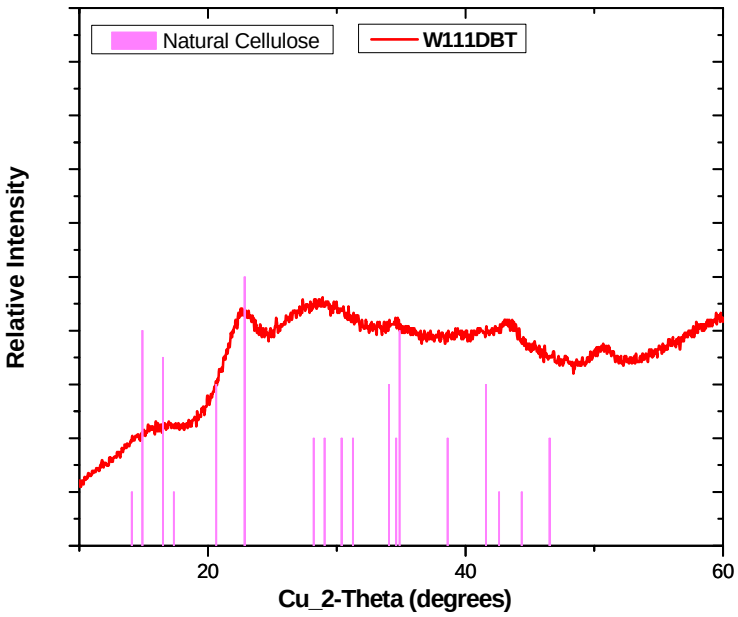

Figure 33. XRD patterns of MG-A subsample 37d reference to natural cellulose.

Mössbauer Results

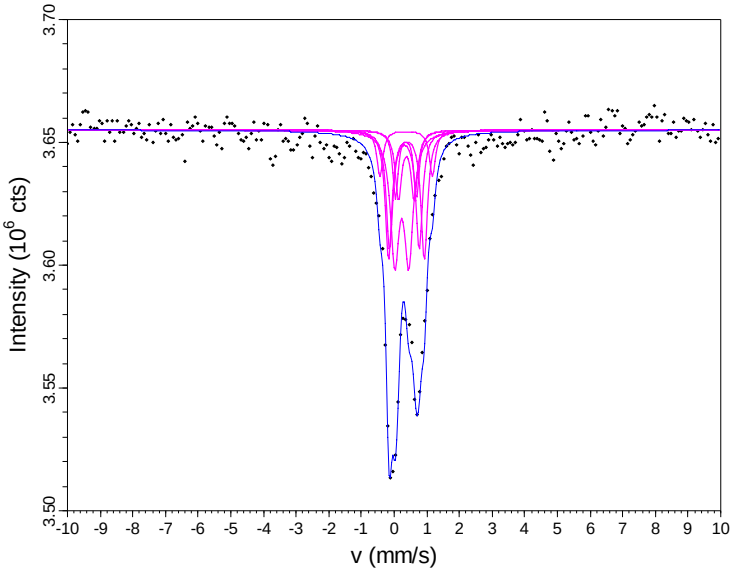

Figure 34. Mössbauer spectrum (300°K) of MG-A subsample 37d.

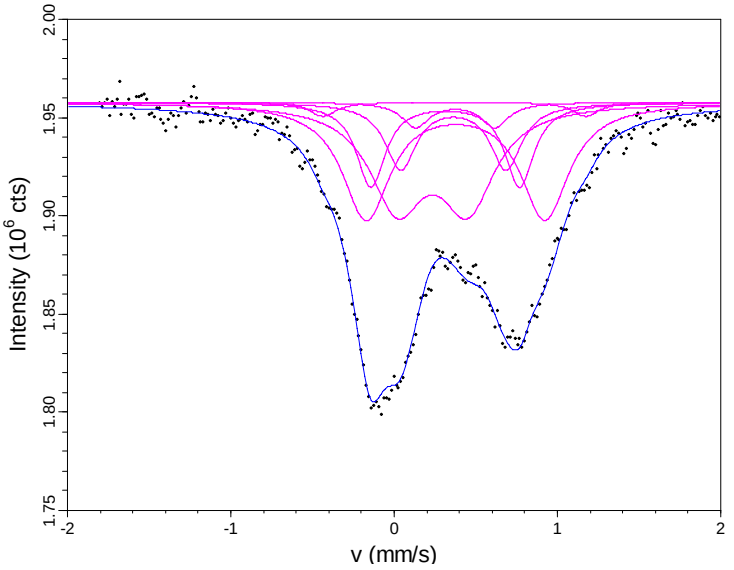

Figure 35. Mössbauer spectrum (300 °K, low velocity) of MG-A subsample 37d.

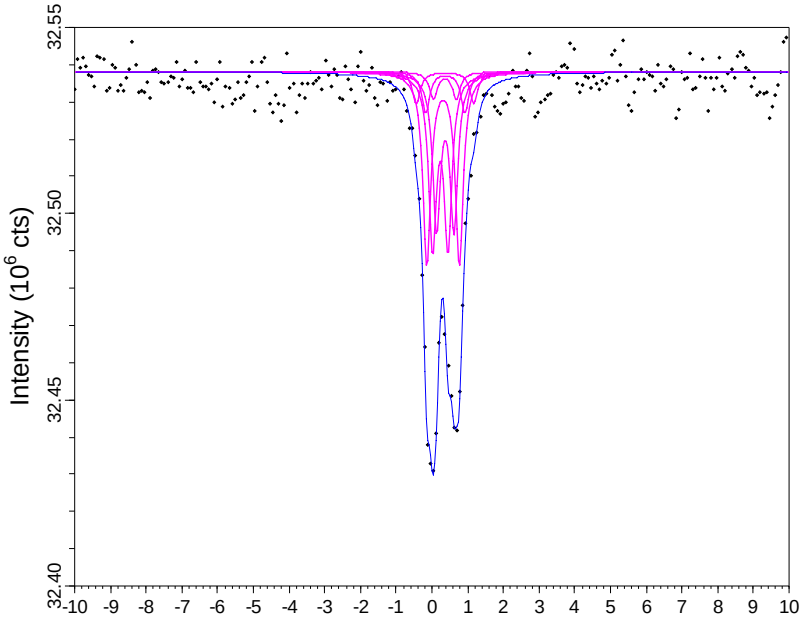

Figure 36. Mössbauer spectrum (300°K) of MG-B subsample 1d.

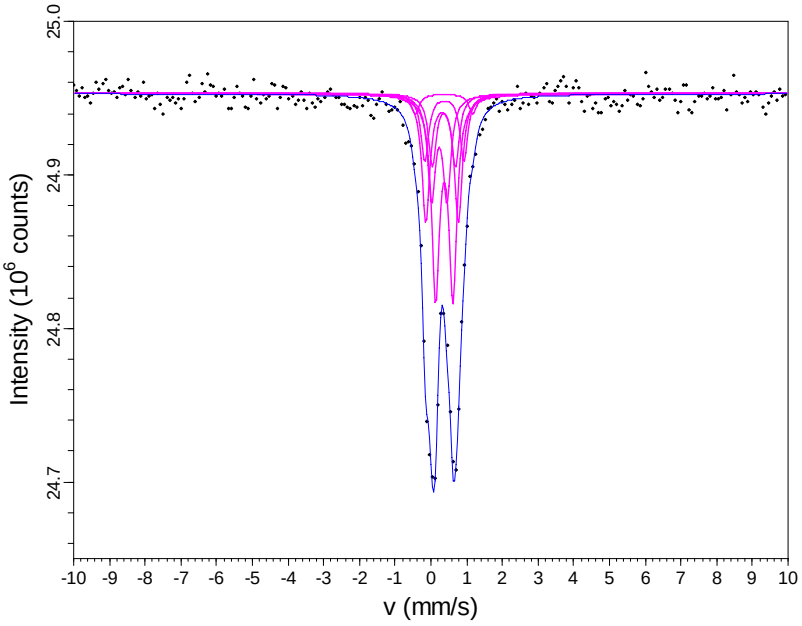

Figure 37. Mössbauer spectrum (300°K) of MG-B subsample 4d.

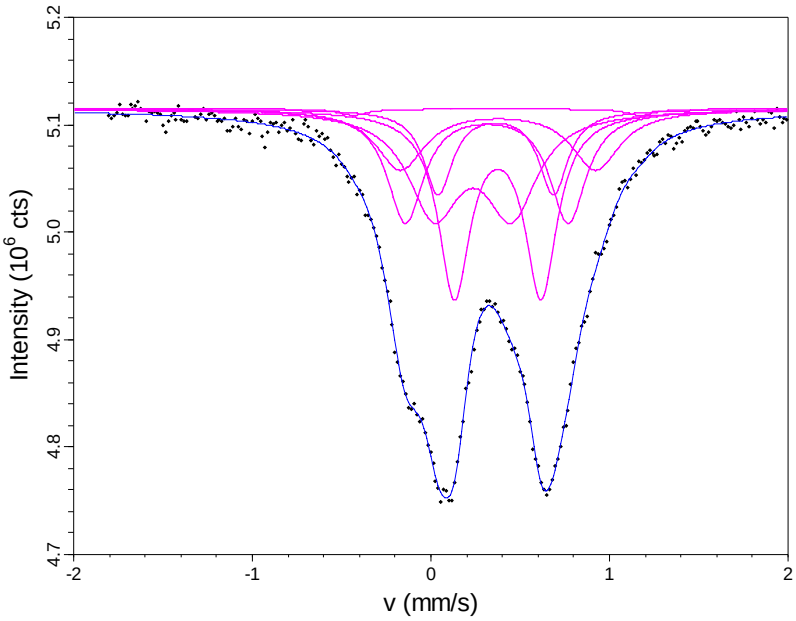

Figure 38. Mössbauer spectrum (300°K, low velocity) of wood MG-B subsample 4d.

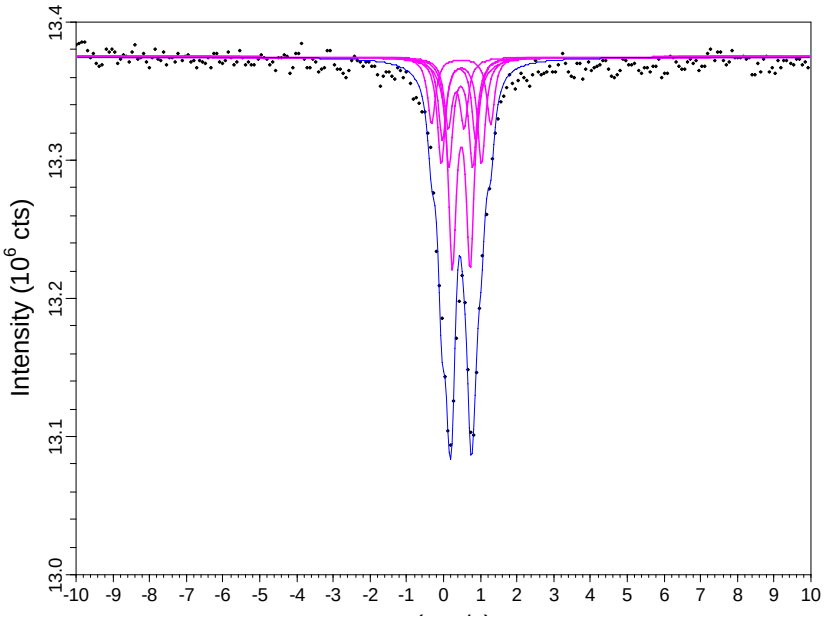

Figure 39. Mössbauer spectrum (77°K) of MG-B subsample 4d.

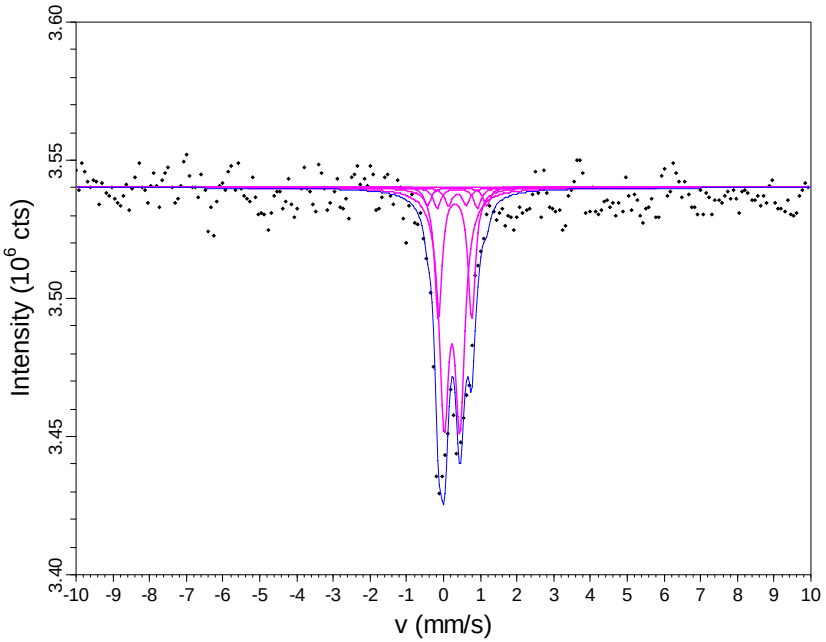

Figure 40. Mössbauer spectrum (300°K) of MD subsample 75d**.**

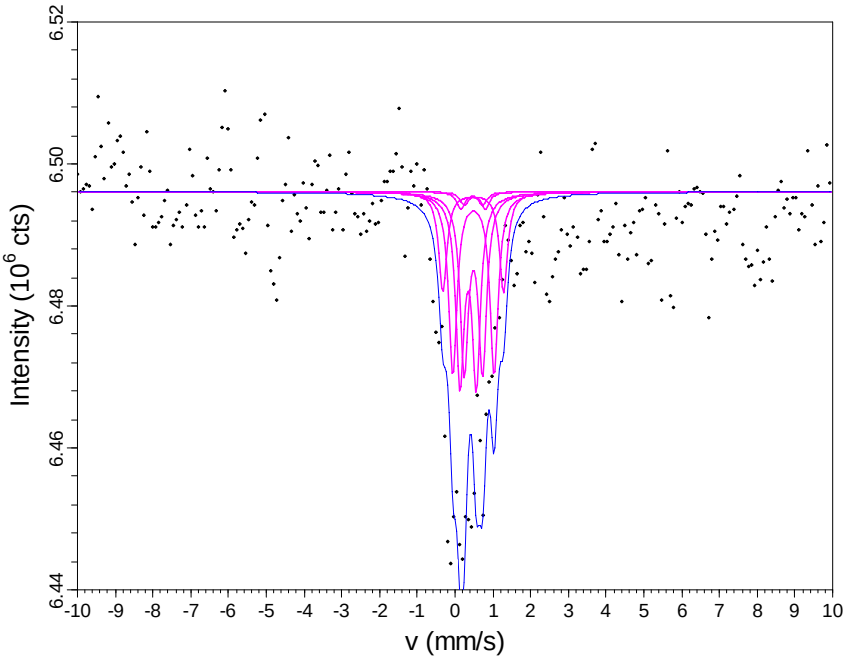

Figure 41. Mössbauer spectrum (77°K) of MD subsample wood 75d.

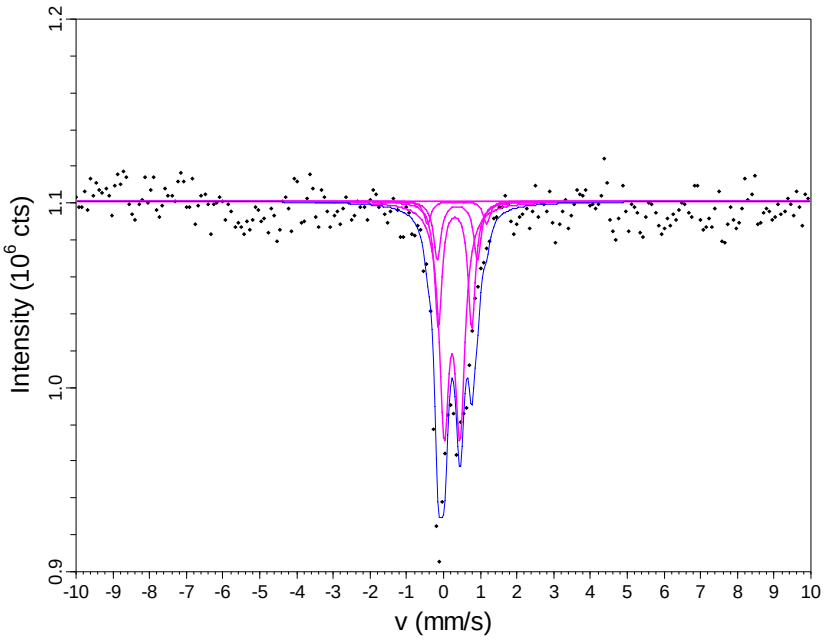

Figure 42. Mössbauer spectrum (300°K) of MD subsample 80d.

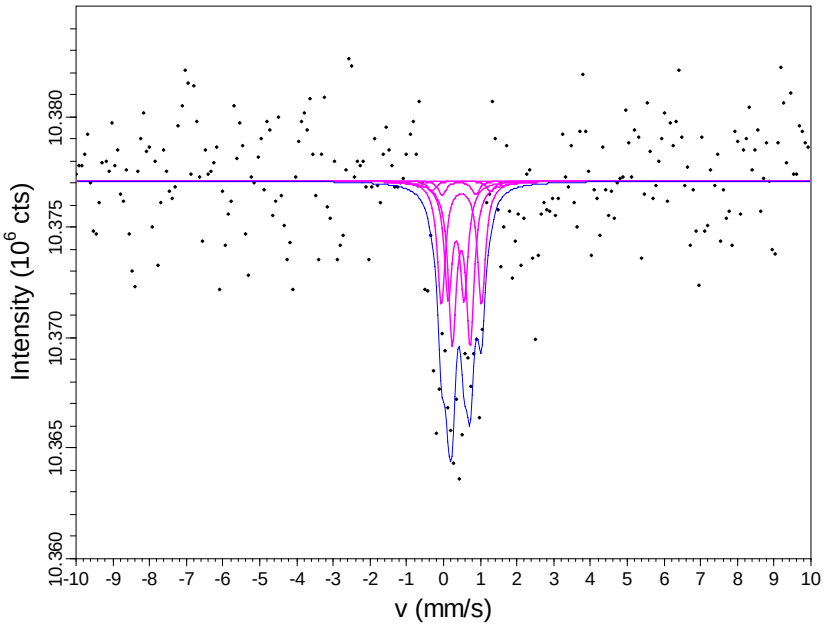

Figure 43. Mössbauer spectrum (77°K) of MD subsample 80d.

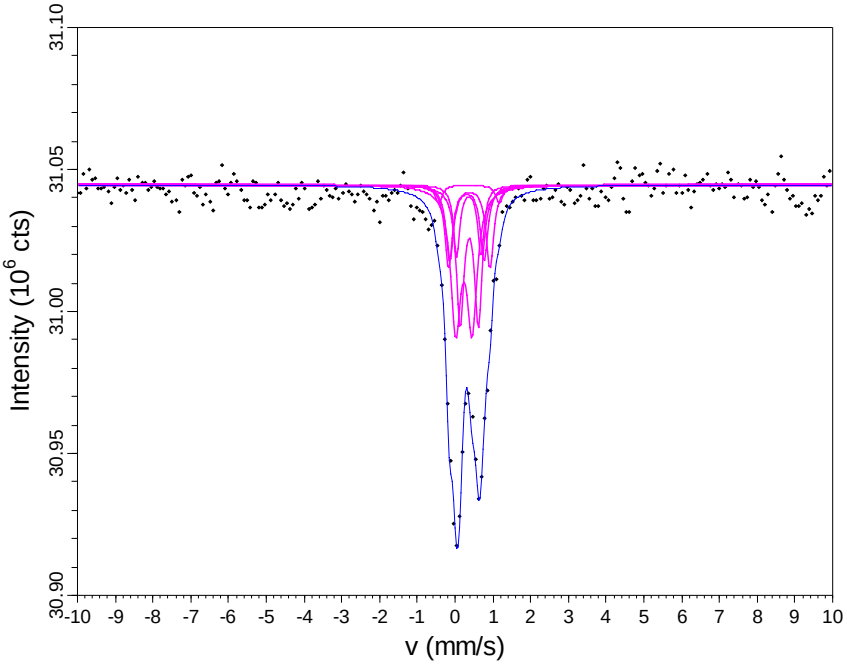

Figure 44. Mössbauer spectrum (300°K) of MD subsample 84d.

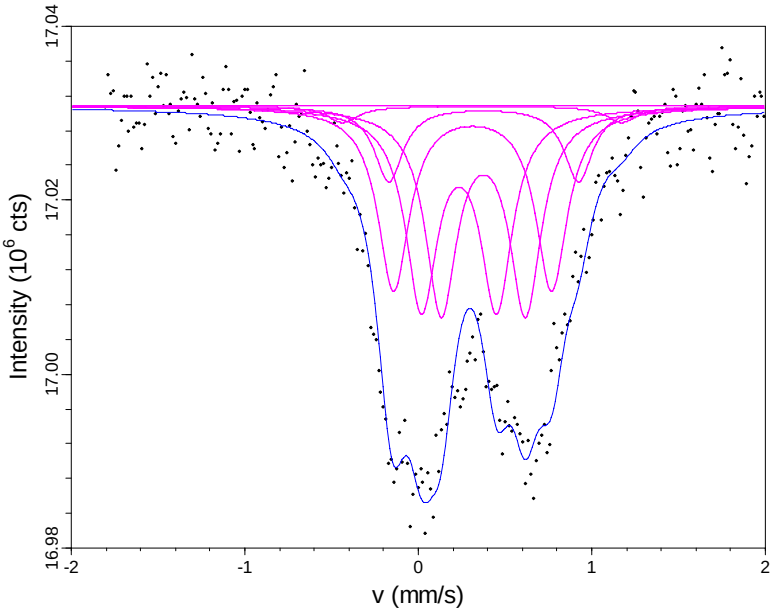

Figure 45. Mössbauer Spectrum (300°K) of MG-B subsample 8d.

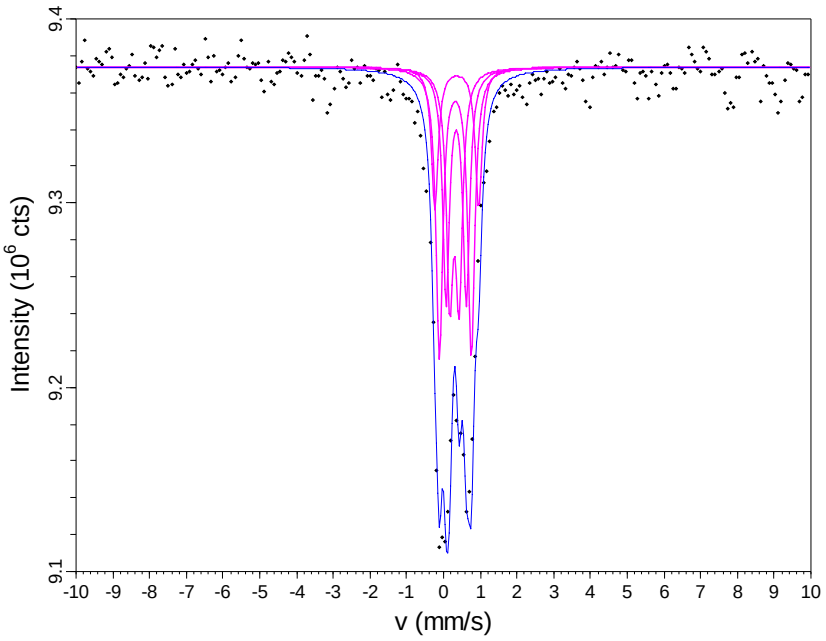

Figure 46. Mössbauer spectrum (300^{o}K, low velocity) of MG-B subsample 8d.

Appendix V: Images of Samples

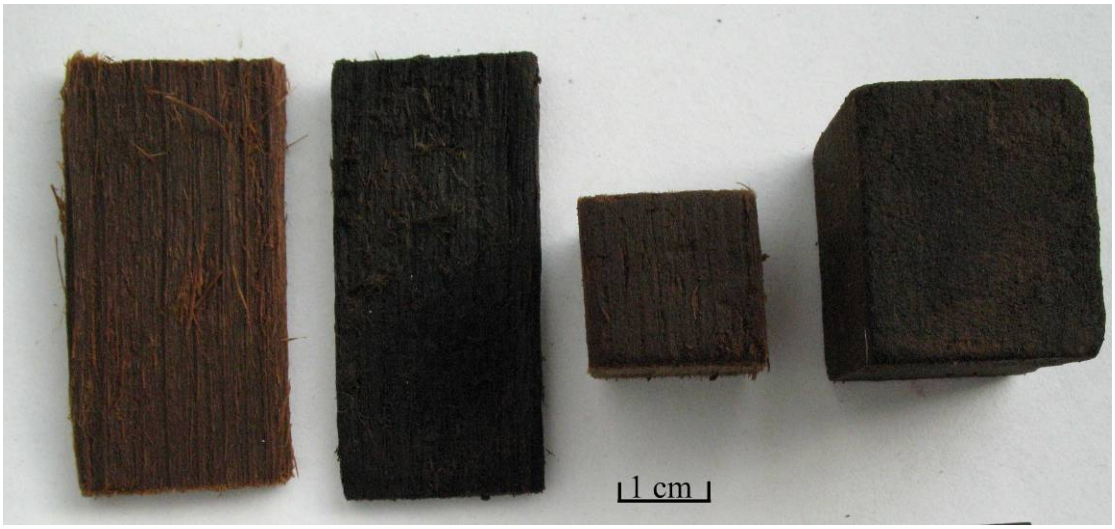

Figure 47. Representative sample types before treatment. Left to right- MD plank, MG-A plank, MD block, MG-B block.

Figure 48. Treated MG-A planks. Left to right- air-dried sample 30d, freeze-dried sample 43a, supercitical-dried sample 30a.

Figure 49. Treated MG-B blocks. Left to right- air-dried sample 17, freeze-dried sample 6, supercitical-dried sample 3.

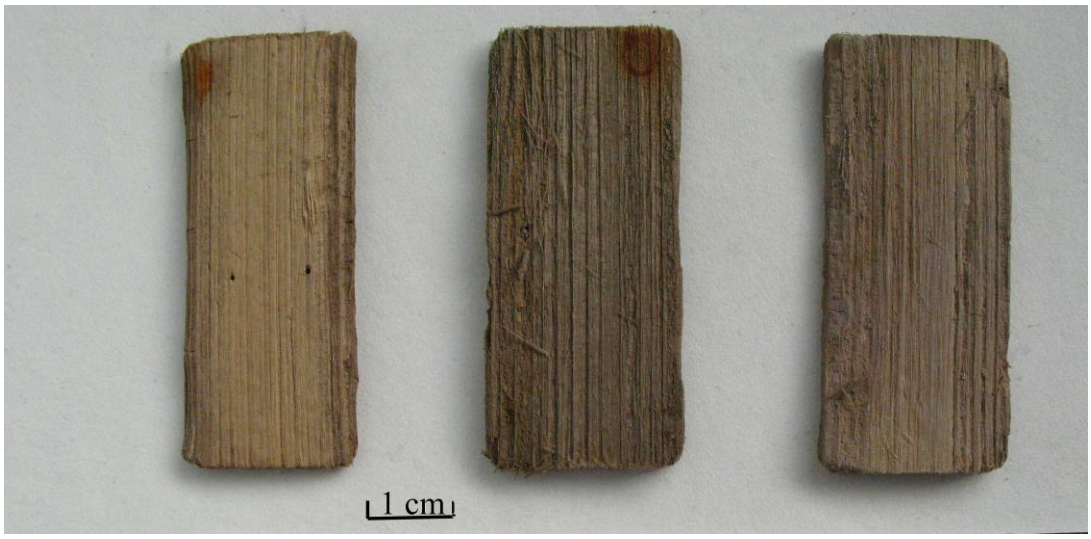

Figure 50. Treated MD planks. Left to right- air-dried sample 48b, freeze-dried sample 48c, supercritical-dried sample 48a.

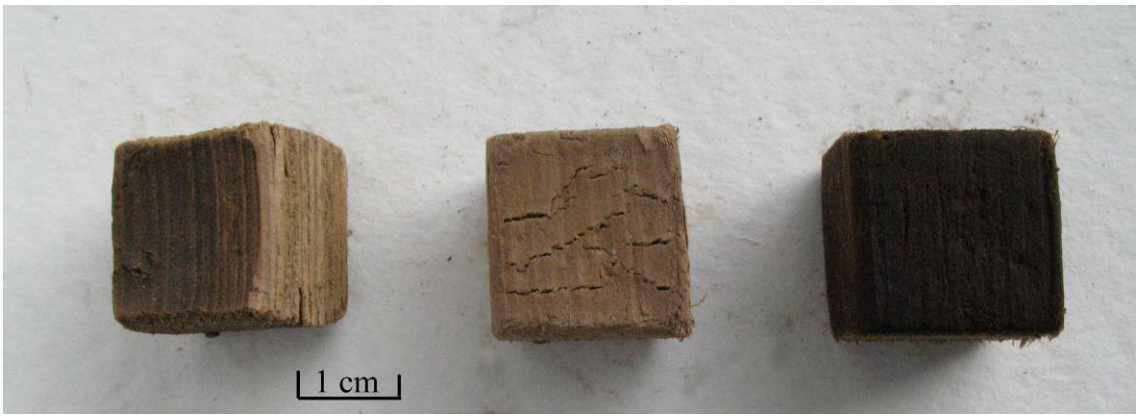

Figure 51. Treated MD blocks. Left to right- air-dried sample 83, freeze-dried sample 88, supercritical-dried sample 87.

Appendix VI: Shrinkage Results

MG-B Blocks	ID	α_r (%)	α_t (%)	α_v (%)	ASE_r (%)	ASE_t (%)	ASE_v (%)
Air-dried	7	23.7	60.2	80.5			
	14	28.4	59.2	80.5			
	17	19.7	52.3	80.6			
Average		23.9	57.2	80.5			
freeze-dried	9	2.2	8.8	11.1	91	85	86
	6	0.3	9.6	11.4	99	83	86
	5	2.0	11.7	11.6	92	80	86
Average		1.5	10.0	11.4	94	83	86
sc-dried	2	2.5	2.3	14.8	90	96	82
	3	5.5	-1.4	16.7	77	102	79
	12	0.5	4.5	14.8	98	92	82
Average		2.8	1.8	15.4	88	97	81

Table 6. MG-B block shrinkage.

MD Blocks	ID	β_r (%)	β_t (%)	β_v (%)	ASE_r (%)	ASE_t (%)	ASE_v (%)
Air-dried	82	5.2	8.9	22.8			
	74	4.5	8.2	18.6			
	86	4.4	8.1	22.5			
Average		4.7	8.4	21.3			
freeze-dried	88	1.0	3.0	1.8	80	64	91
	79	-2.0	2.3	0.4	142	73	98
	83	-0.1	0.0	1.1	102	100	95
Average		-0.4	1.7	1.1	108	79	95
sc-dried	87	2.4	8.2	9.9	50	3	54
	85	2.7	7.4	10.1	43	11	53
	89	2.4	3.5	11.9	48	58	44

Table 7. MD block shrinkage.

MD Planks	ID	β_r (%)	β_v (%)	ASE_r (%)	ASE_v (%)
Air-dried	48b	3.8	22.3		
	49d	3.0	21.4		
	49e	3.2	27.6		
Average		3.3	23.8		
freeze-dried	48c	0.2	3.4	94	86
	49c	2.0	10.8	84	54
	49f	0.4	3.8	97	84
Average		0.9	6.0	92	75
sc-dried	48a	0.5	10.7	86	55
	49b	2.0	9.6	39	60
	49a	-0.3	9.3	109	61
Average		0.7	9.9	78	58

Table 8. MD plank shrinkage.

MG-A Planks	ID	β_r (%)	β_v (%)	ASE_r (%)	ASE_v (%)
Air-dried	43b	5.4	38.2		
	30g	19.9	25.7		
	30d	12.5	43.7		
Average		12.6	35.9		
freeze-dried	40b	split			
	43a	1.8	1.7	86	95
	40f	3.1	7.3	76	80
Average		2.4	4.5	81	88
sc-dried	30a	0.7	2.7	94	93
	40c	split			
	36a	0.0	9.3	100	74
Average		0.3	6.0	97	83

Table 9. MG-A plank shrinkage.

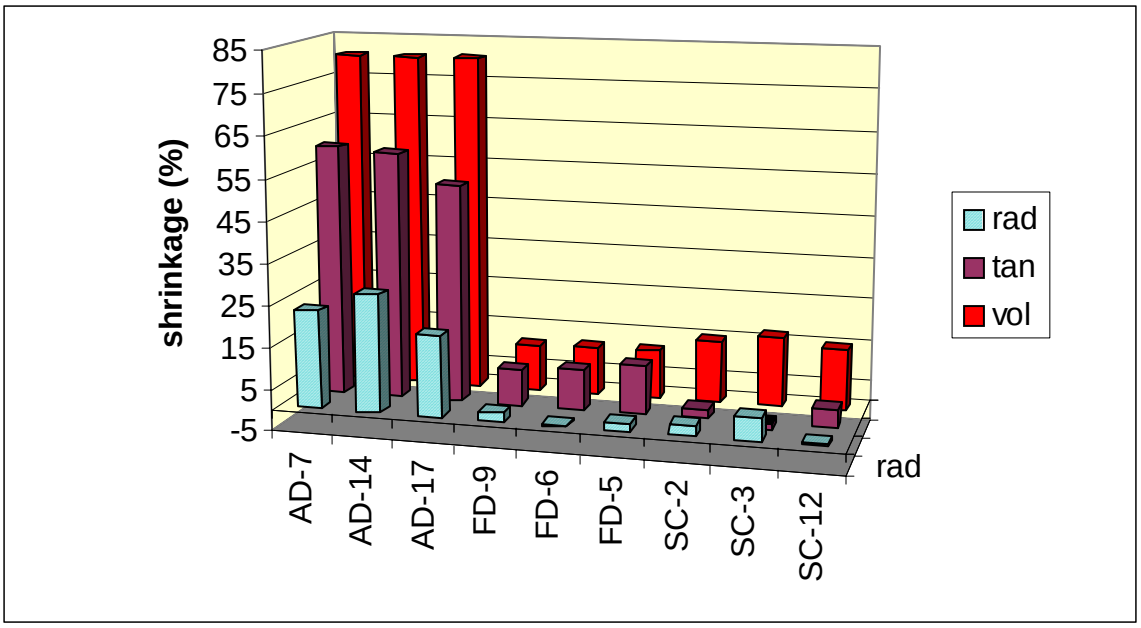

Figure 52. Comparison of radial, tangential and volumetric shrinkage of MG-B blocks. X axis denotes sample ID number preceded by type of treatment- AD is air-dried; FD is freeze-dried; SC is supercritical-dried**.**

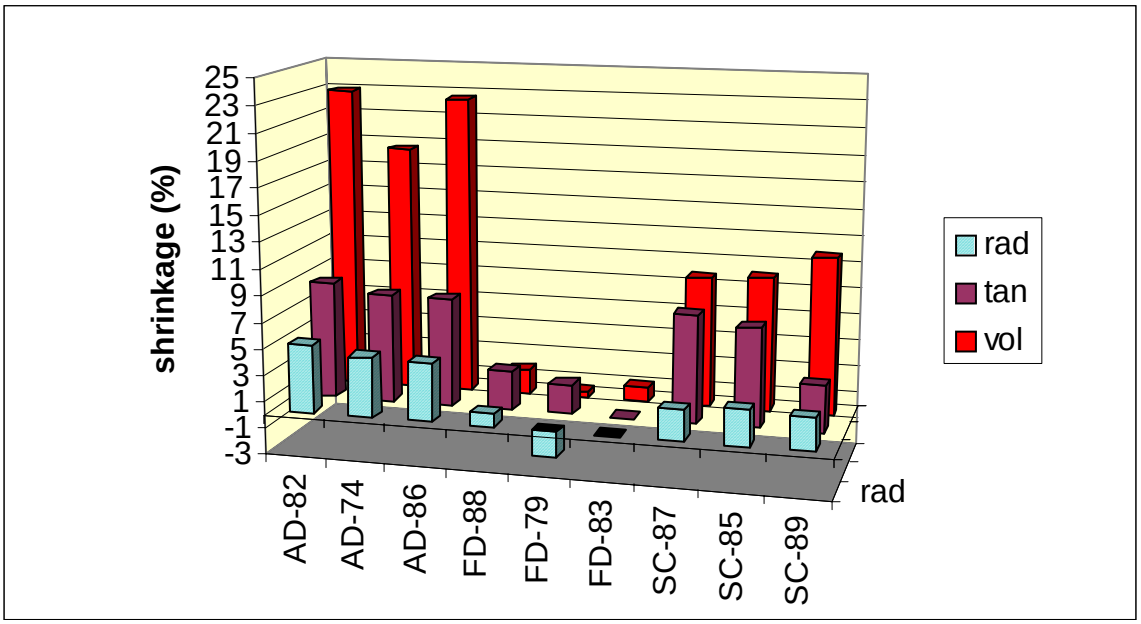

Figure 53. Comparison of radial, tangential and volumetric shrinkage of MD blocks. X axis denotes sample ID number preceded by type of treatment- AD is air-dried; FD is freeze-dried; SC is supercritical-dried**.**

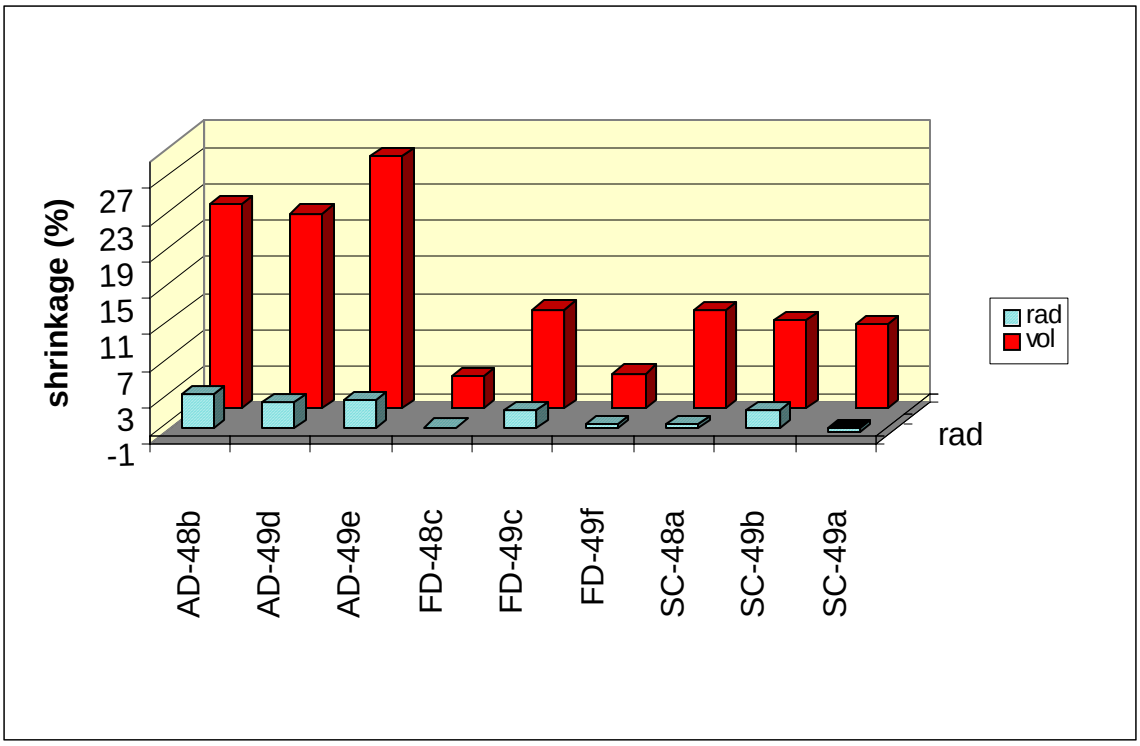

Figure 54. Comparison of radial and volumetric shrinkage of MD planks. X axis denotes sample ID number preceded by type of treatment- AD is air-dried; FD is freeze-dried; SC is supercritical-dried**.**

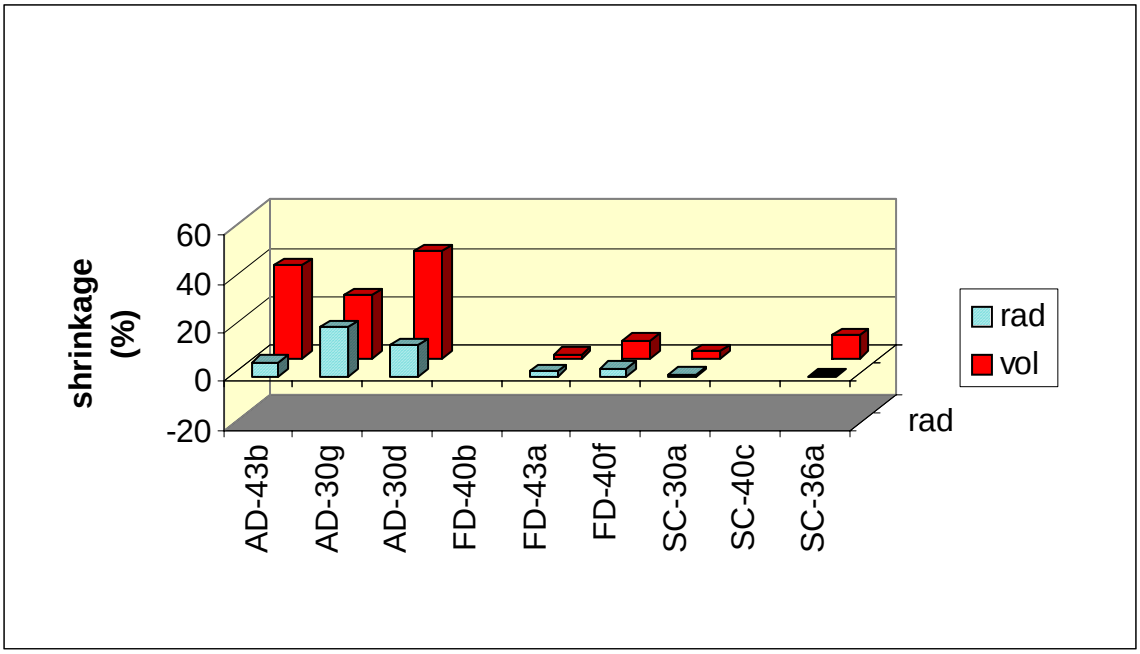

Figure 55. Comparison of radial and volumetric shrinkage of MG-A planks. X axis denotes sample ID number preceded by type of treatment- AD is air-dried; FD is freeze-dried; SC is supercritical-dried**.**

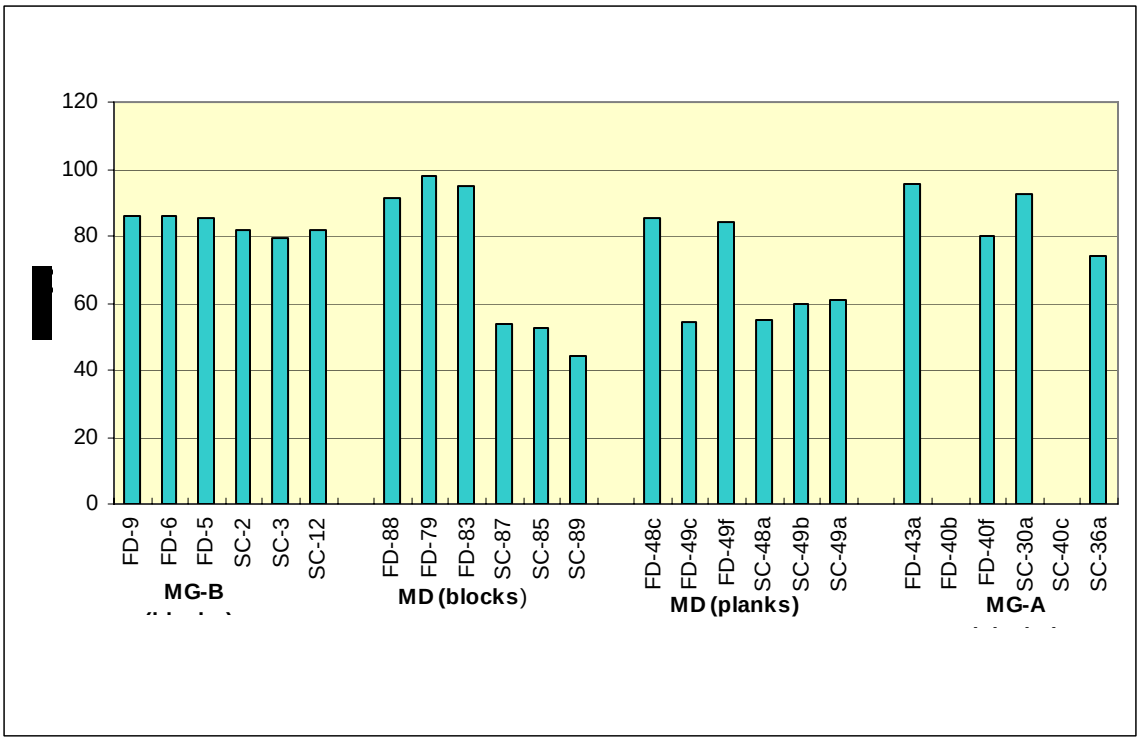

Figure 56. Comparison of anti-shrink efficiency values for all samples. X axis denotes sample ID number preceded by type of treatment- AD is air-dried; FD is freeze-dried; SC is supercritical-dried

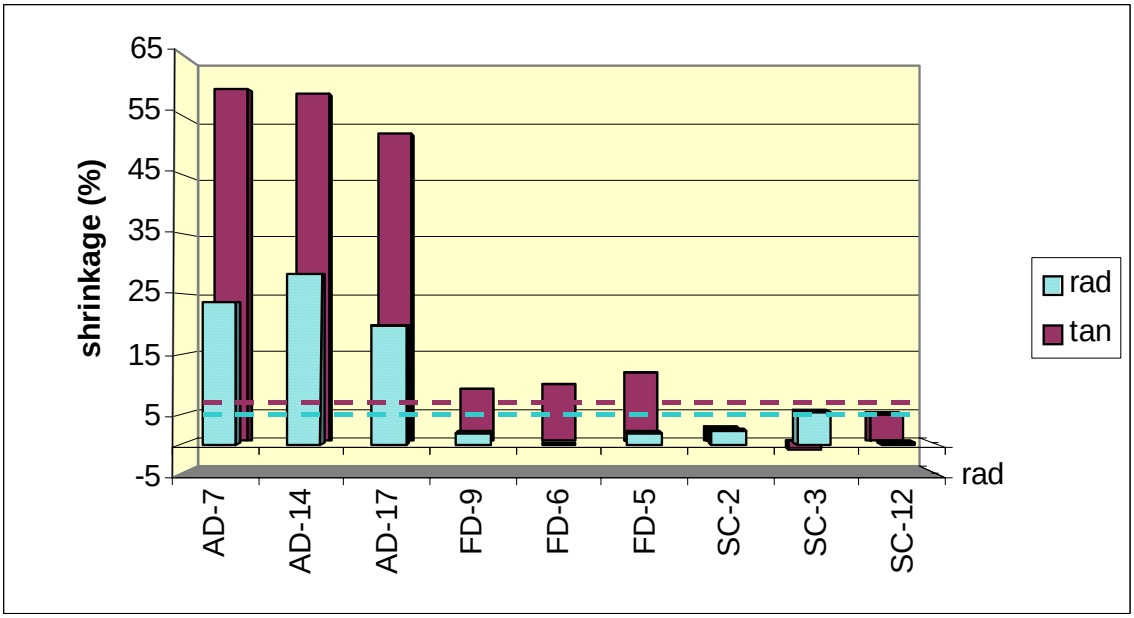

Figure 57. Tangential and radial shrinkage of MG-B blocks with expected normal shrinkage- purple dashed line is expected β_t and blue dashed line is β_r. X axis denotes sample ID number preceded by type of treatment- AD is air-dried; FD is freeze-dried; SC is supercritical-dried**.**

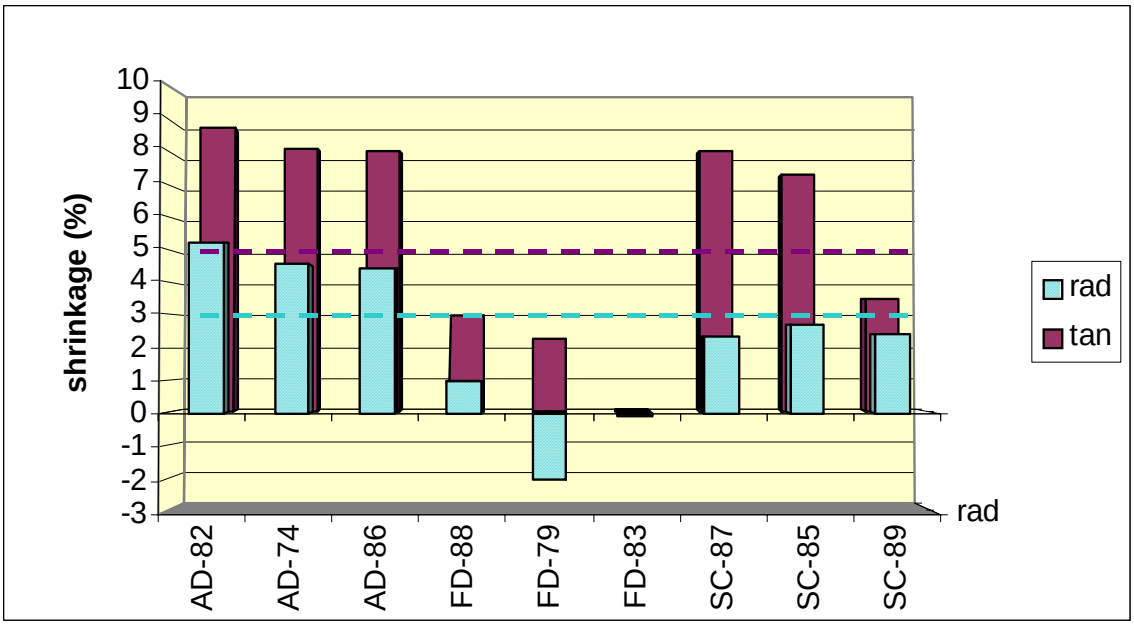

Figure 58. Tangential and radial shrinkage of MD blocks with expected normal shrinkage- purple dashed line is expected β_t and blue dashed line is β_r. X axis denotes sample ID number preceded by type of treatment- AD is air-dried; FD is freeze-dried; SC is supercritical-dried**.**

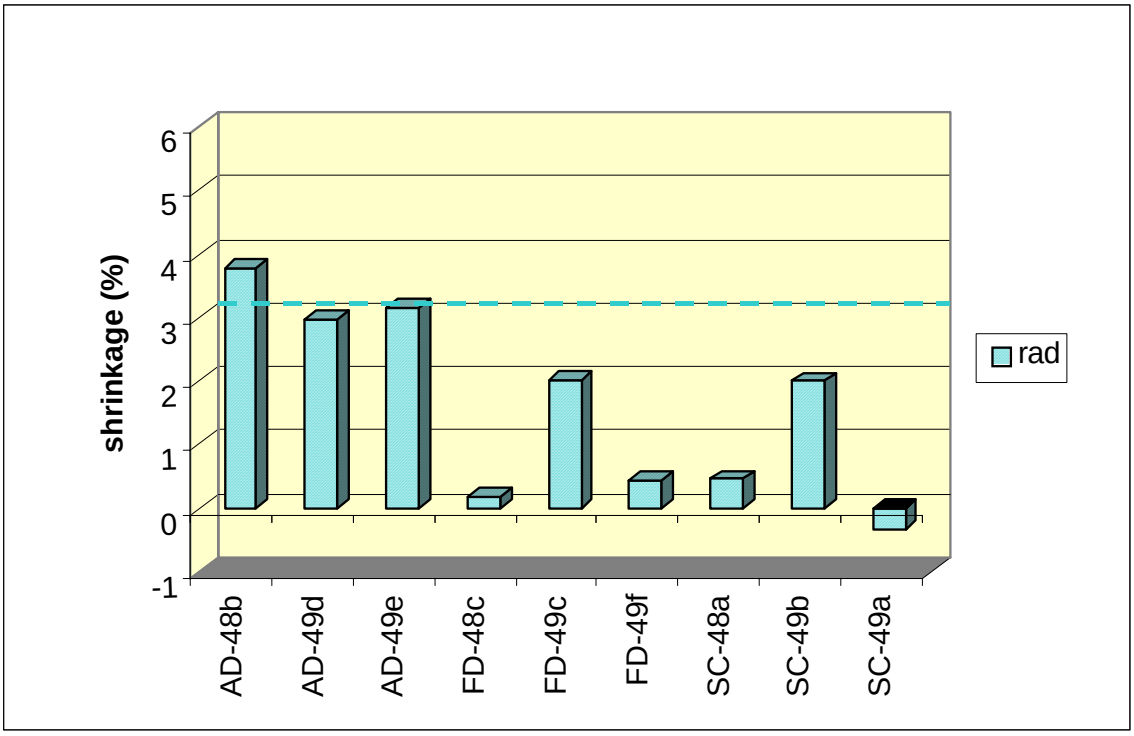

Figure 59. Radial shrinkage of MD planks with expected normal shrinkage- blue dashed line. X axis denotes sample ID number preceded by type of treatment- AD is air-dried; FD is freeze-dried; SC is supercritical-dried**.**

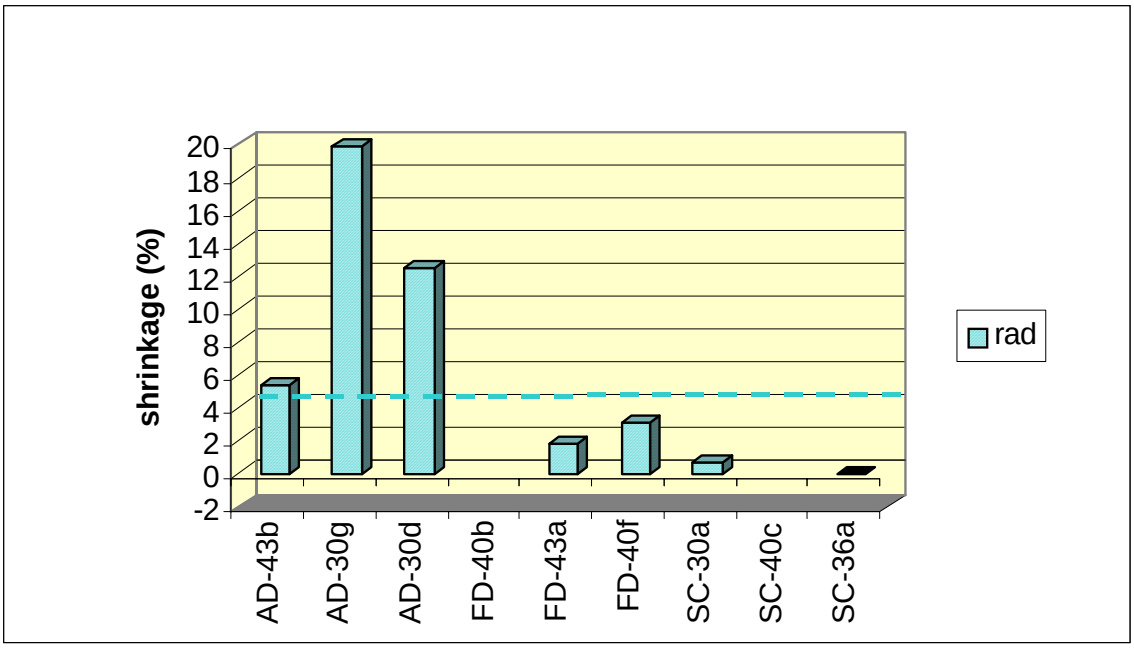

Figure 60 Radial shrinkage of MG-A planks with expected normal shrinkage- blue dashed line. X axis denotes sample ID number preceded by type of treatment- AD is air-dried; FD is freeze-dried; SC is supercritical-dried**.**

Appendix VII: 3D Models

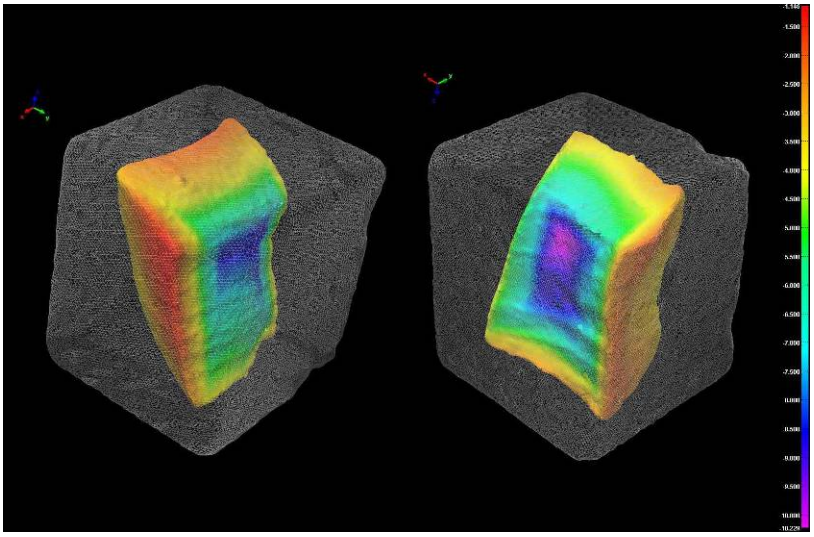

Figure 61. 3D comparison model of air-dried MG-B block 17- front and back. The grey wire frame model is the wet sample and the colored solid model is the treated sample. Scale is in microns**.**

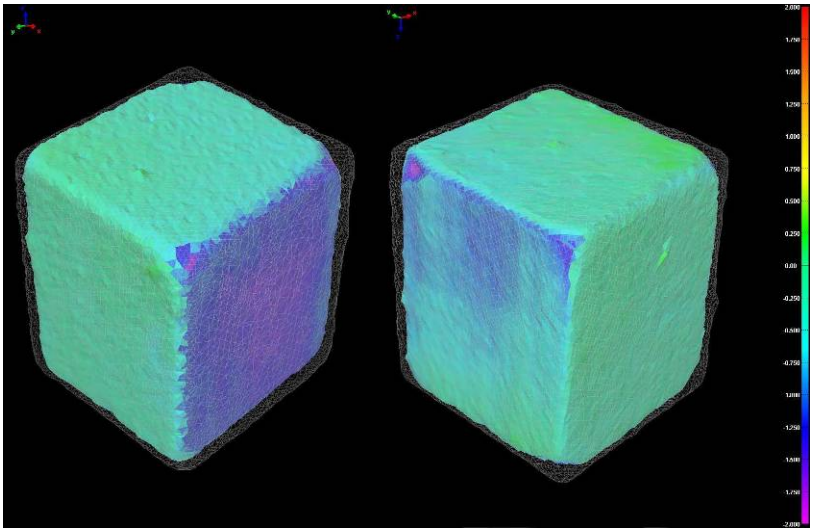

Figure 62. 3D comparison model of freeze-dried MG-B block 6- front and back. The grey wire frame model is the wet sample and the colored solid model is the treated sample. Scale is in microns.

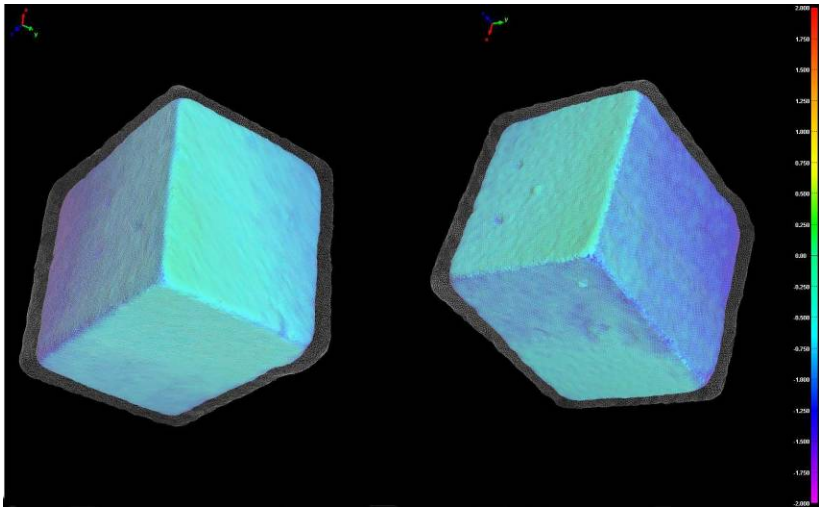

Figure 63 3D comparison model of supercritical-dried MG-B block 3- front and back. The grey wire frame model is the wet sample and the colored solid model is the treated sample. Scale is in microns.

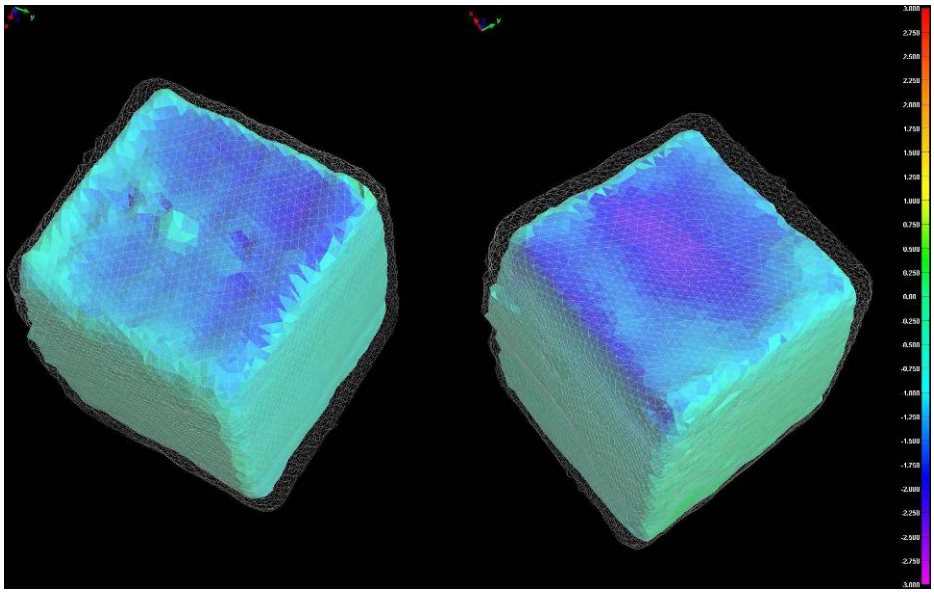

Figure 64. 3D comparison model of air-dried MD block 83- front and back. The grey wire frame model is the wet sample and the colored solid model is the treated sample. Scale is in microns.

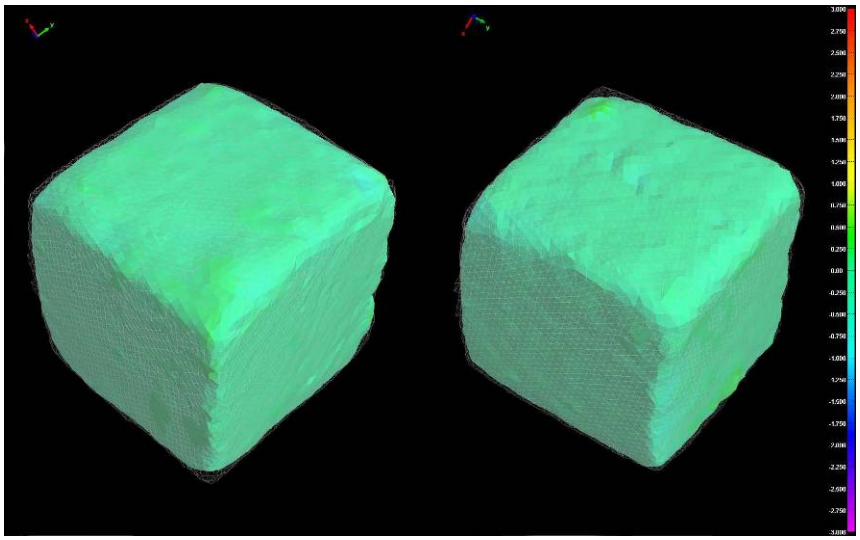

Figure 65. 3D comparison model of freeze-dried MD block 88- front and back. The grey wire frame model is the wet sample and the colored solid model is the treated sample. Scale is in microns.

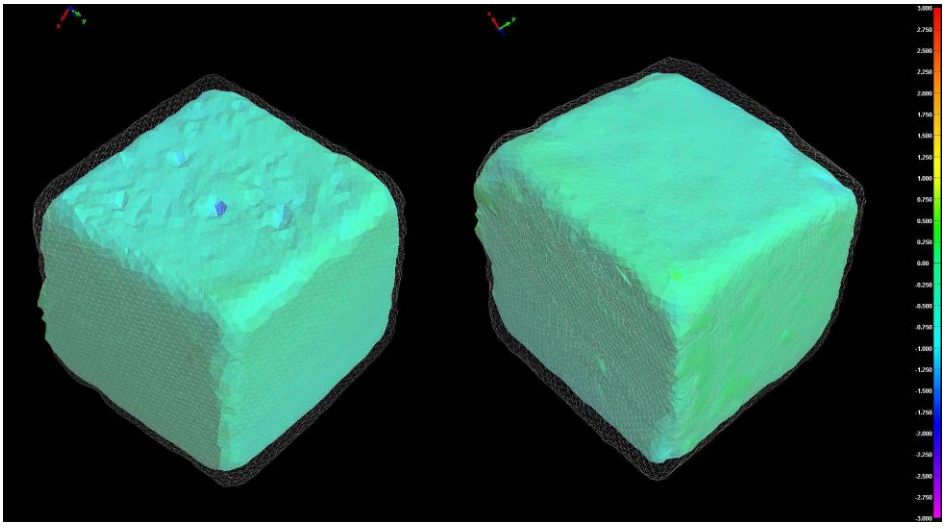

Figure 66. 3D comparison model of supercritical-dried MD block 87- front and back. The grey wire frame model is the wet sample and the colored solid model is the treated sample. Scale is in microns.

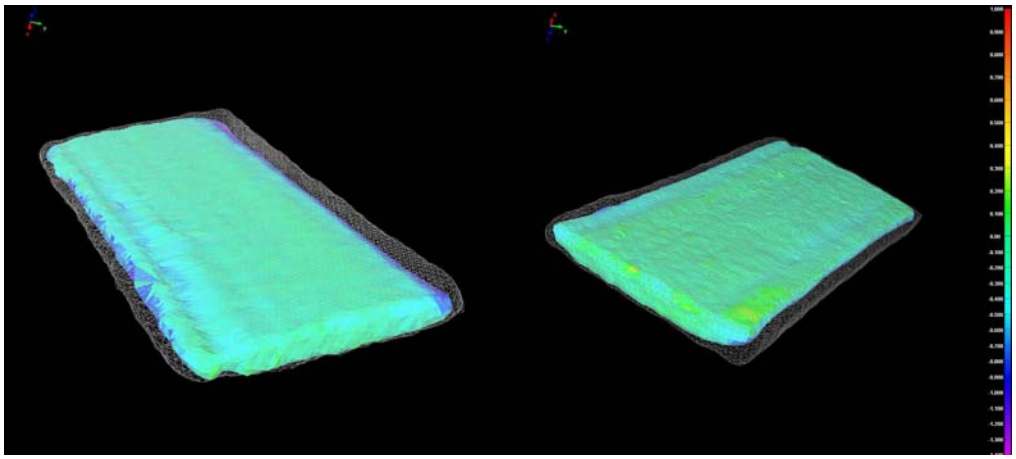

Figure 67. 3D comparison model of air-dried MD plank 48b- front and back. The grey wire frame model is the wet sample and the colored solid model is the treated sample. Scale is in microns.

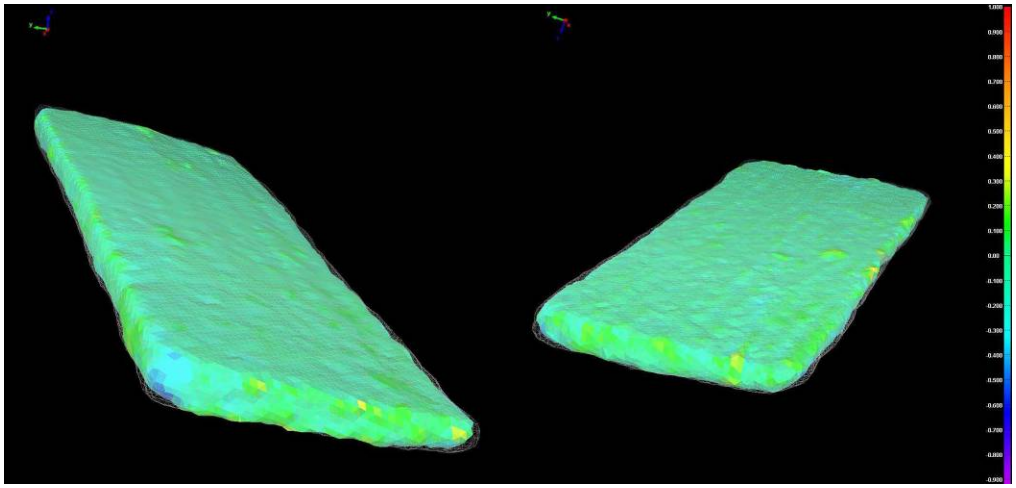

Figure 68. 3D comparison model of freeze-dried MD plank 48c- front and back. The grey wire frame model is the wet sample and the colored solid model is the treated sample. Scale is in microns.

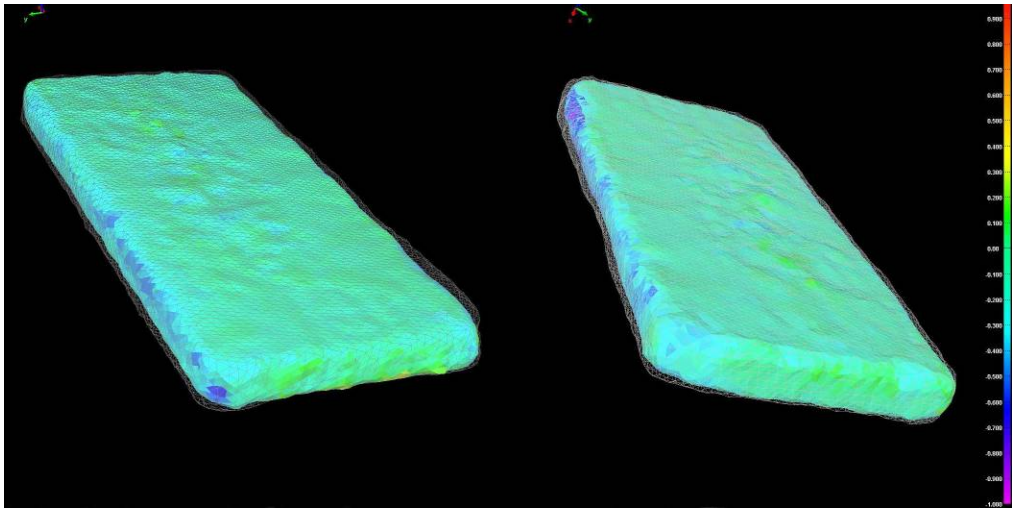

Figure 69. 3D comparison model of supercritical-dried MD plank 49b- front and back. The grey wire frame model is the wet sample and the colored solid model is the treated sample. Scale is in microns**.**

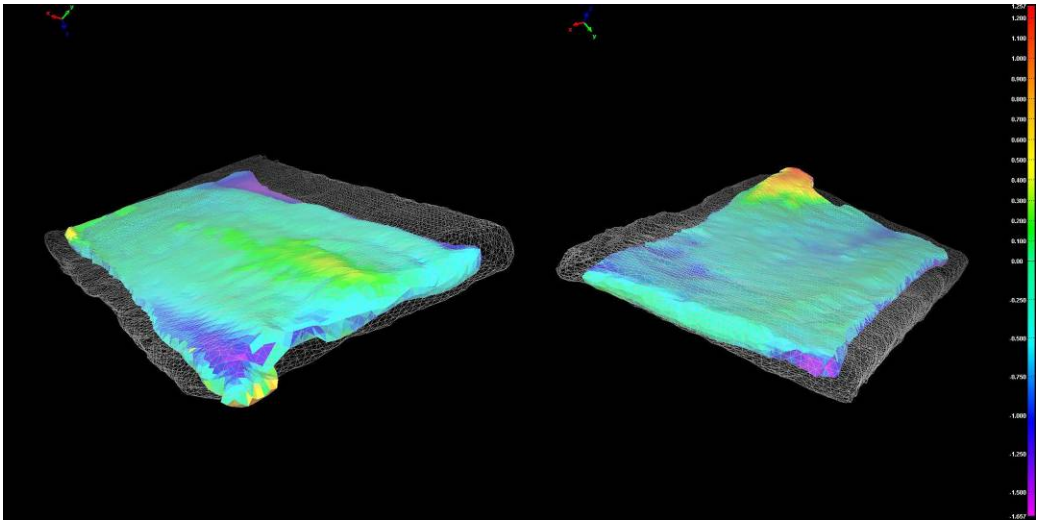

Figure 70. 3D comparison model of air-dried MG-A plank 30d- front and back. The grey wire frame model is the wet sample and the colored solid model is the treated sample. Scale is in microns.

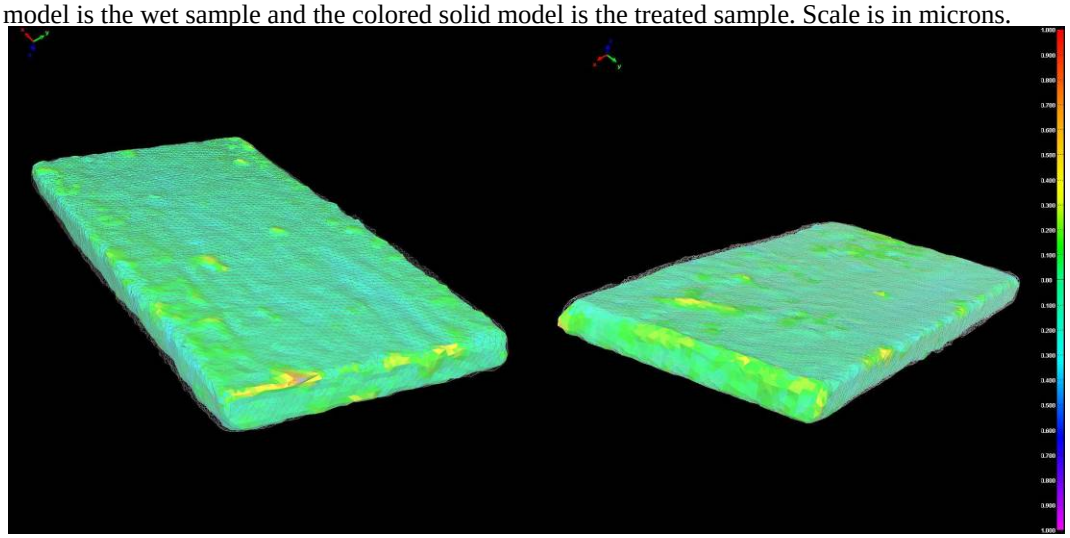

Figure 71. 3D comparison model of freeze-dried MG-A plank 43a- front and back. The grey wire frame model is the wet sample and the colored solid model is the treated sample. Scale is in microns.

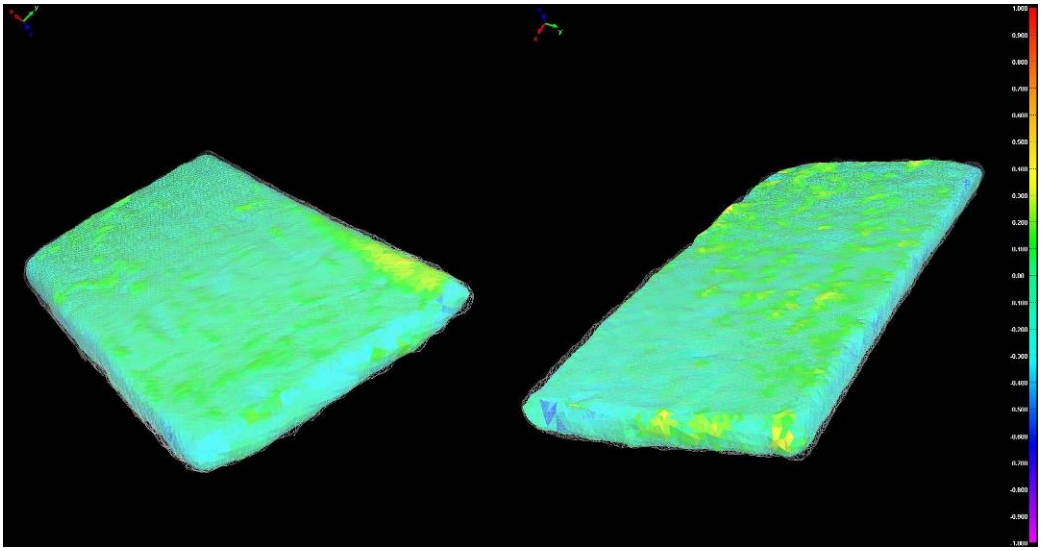

Figure 72. 3D comparison model of supercritical-dried MG-A plank 30a- front and back. The grey wire frame model is the wet sample and the colored solid model is the treated sample. Scale is in microns.